AFRL-OSR-VA-TR-2014-0186

MULTIFUNCTIONAL FLEXIBLE COMPOSITES BASED ON CONTINUOUS CARBON NANOTUBE FIBERS

TSU-WEI CHOU
UNIVERSITY OF DELAWARE

08/07/2014
Final Report

Air Force Research Laboratory
AF Office Of Scientific Research (AFOSR)/ RTD
Arlington, Virginia 22203
Air Force Materiel Command

REPORT DOCUMENTATION PAGE

Form Approved
OMB No. 0704-0188

1. REPORT DATE *(DD-MM-YYYY)*	**2. REPORT TYPE**	**3. DATES COVERED** *(From - To)*
7/28/14	Final Report	7/1/11 - 6/30/14

4. TITLE AND SUBTITLE

Multifunctional Flexible Composites Based on Continuous Carbon Nanotube Fiber

5a. CONTRACT NUMBER

5b. GRANT NUMBER
FA9550-11-1-0124

5c. PROGRAM ELEMENT NUMBER

6. AUTHOR(S)

Tsu-Wei Chou, Yuntian T. Zhu

5d. PROJECT NUMBER

5e. TASK NUMBER

5f. WORK UNIT NUMBER

7. PERFORMING ORGANIZATION NAME(S) AND ADDRESS(ES)

UNIVERSITY OF DELAWARE
OFFICE OF THE VICE PROVOST FOR RESEARCH
220 HULLIHEN HALL
NEWARK, DE 19716-0099

8. PERFORMING ORGANIZATION REPORT NUMBER

FINAL-1

9. SPONSORING / MONITORING AGENCY NAME(S) AND ADDRESS(ES)

AF Office of Scientific Research
875 N. Randolph St. Room 3112
Arlington, VA 22203

10. SPONSOR/MONITOR'S ACRONYM(S)

AFOSR

11. SPONSOR/MONITOR'S REPORT NUMBER(S)

12. DISTRIBUTION / AVAILABILITY STATEMENT

Approved for Public Release; distribution is Unlimited.

13. SUPPLEMENTARY NOTES

14. ABSTRACT

Continuous carbon nanotube fibers possess high mechanical properties and electrical conductivity, demonstrating the potential of multifunctional applications in various fields. With the support of the Project "Multifunctional Flexible Composites Based on Continuous Carbon Nanotube Fiber" (grant No. FA9550-11-1-0124), we systematically studied the synthesis and properties of dry-spun CNT fibers with different spinning techniques, including the tensile strength, compressive strength, microstructure evolution, torsional behavior, electromechanical response, failure behavior, and tensile stress relaxation behavior. The potential use of CNT fiber for torsional sensors have been demonstrated. The interfacial behaviors between CNT fibers and graphene film, PDMS, epoxy resins have also been examined. Molecular dynamics simulations of the fiber structural evolution from CNT array to film to fiber and the resulting mechanical behavior were conducted to gain insight into the fundamental strengthening mechanisms. To demonstrate the multifunctional applications of CNT fiber, we further designed and fabricated transparent, stretchable conductors based on CNT fibers and PDMS. Finally, the synthesis and electromechanical behavior of graphene based continuous fibers,

15. SUBJECT TERMS

Carbon nanotube fiber, graphene fiber, synthesis, characterization, electro-mechanical property, damage sensing, flexible compo

16. SECURITY CLASSIFICATION OF:			**17. LIMITATION OF ABSTRACT**	**18. NUMBER OF PAGES**	**19a. NAME OF RESPONSIBLE PERSON**
a. REPORT	**b. ABSTRACT**	**c. THIS PAGE**			Tsu-Wei Chou
U	U	U	UU	45	**19b. TELEPHONE NUMBER** *(include area code)* 302-831-1550

AFOSR FINAL REPORT

Principal Investigator:

Tsu-Wei Chou
Pierre S. du Pont Chair of Engineering
Department of Mechanical Engineering
University of Delaware, Newark, DE 19716
Phone: 302-831-1550/2904; Fax: 302-831-3619
E-mail: chou@udel.edu

Co-Principal Investigator:

Yuntian T. Zhu
Distinguished Professor of Materials Science & Engineering
Department of Materials Science & Engineering
North Carolina State University
Raleigh, NC 27695-7919
Phone: 919 -513-0559; Fax: 919-515-3419
Email: ytzhu@ncsu.edu

Project Title:

Multifunctional Flexible Composites Based on Continuous Carbon Nanotube Fiber

Grant No:

FA9550-11-1-0124

Period of Performance:

July 1, 2011 - June 30, 2014

Part I: Report by the Principal Investigator

1. Introduction

The following research has been conducted during the grant period.

Year 1:

(1) The electromechanical response and failure behavior of pure carbon nanotube (CNT) fibers and CNT composite fibers under tensile loading were characterized through single fiber tensile tests. See section 2.1.

(2) The interfacial behavior of CNT fiber/epoxy composites were characterized using micro-droplet tests. The effective CNT fiber/epoxy interfacial shear strength was found to be 14.4 MPa. See section 2.2.

(3) The entanglements in CNT fibers were investigated by using a self-folded nanotube model. The tensile behavior of the self-folded CNT has been examined by using both the approximate theoretical model and atomistic simulations. See section 2.3.

(4) The opportunities and challenges of state-of-the-art of CNT fibers were reviewed. See section 2.4.

Year 2:

(1) The compressive strengths of pure and composite CNT fibers were obtained as 416 and 573 MPa, respectively, using a tensile recoil measurement. The principal recoil compressive failure mode of pure CNT fiber was kinking, while the CNT epoxy composite fiber exhibited a failure mode in bending with combined tensile and compressive failure morphologies. See section 2.5.

(2) The torsional behavior of CNT fibers was investigated by performing single fiber torsion tests. Bulk shear modulus was obtained as 0.40 ± 0.02 GPa for pure fiber and 2.79 ± 0.64 GPa for resin infused fibers. See section 2.6.

(3) The tensile stress relaxation behavior of CNT fibers was studied. Both the pure CNT fiber and the CNT/epoxy composite fiber exhibited significant stress decay during the relaxation process. See section 2.7.

(4) The strain rate-dependent tensile properties and dynamic electromechanical response of CNT fibers were studied using the Kolsky tension bar methodology. See section 2.8.

(5) A CNT fiber based stretchable conductor was designed and fabricated using the prestraining-then-buckling approach. The CNT fiber/PDMS composite film showed very little variation in resistance under multiple stretching-and-releasing cycles up to a prestrain level of 40%. See section 2.9.

(6) The mechanical behavior and microstructural evolution of CNT fibers under twisting and tension have been investigated using coarse-grained molecular dynamics (CGMD) simulations. See section 2.10.

(7) The state-of-the-art of CNT fibers for advanced composites were reviewed. See section 2.11.

Year 3:

(1) The super-aligned CNT film/graphene hybrid fibers were designed and fabricated. The failure behaviors of fiber under axial tensile loading showed significant correlations with the CNT film thickness and the interfacial nano/micro structures. See section 2.12.
(2) The porous CNT fibers with tunable large pores of hundreds of nanometers in diameter have been synthesized from a commercially available sizing material, their mechanical and electrical properties were studied. See section 2.13.
(3) The electromechanical behaviors of reduced graphene oxide fiber were studied. An immediate and significant modulus decrease upon electric current application was observed and investigated. See section 2.14.
(4) Literature in the synthesis, properties and applications of graphene-based fibers has been reviewed. See section 2.15.

A summary of the research findings are given in the following section.

2. Brief Overview of Accomplishments

During the three-year grant period, various research topics pertaining to the synthesis, characterization, electromechanical and interfacial properties of CNT fibers; synthesis and electromechanical properties of graphene-based fibers; molecular dynamics simulations and multifunctional flexible composite applications of CNT fiber have been explored. Thirteen journal papers reporting the findings have been published; three manuscripts are in various stages of review or preparation. Their contents are summarized below.

2.1 electromechanical response and failure behavior of CNT fibers [1]

The mechanical and electrical behavior of carbon nanotube fibers spun continuously from an aerogel is discussed. These fibers exhibit moderate strength (0.19 GPa) and elastic moduli (9.16 GPa). Their piezoresistive behavior, evaluated through active resistance measurements during tensile loading, demonstrates their potential for sensing applications in advanced composite materials. Insight into the failure behavior of the aerogel-spun fibers is gained through microscopic examination of the failed fibers, as well as analysis of their electrical response.

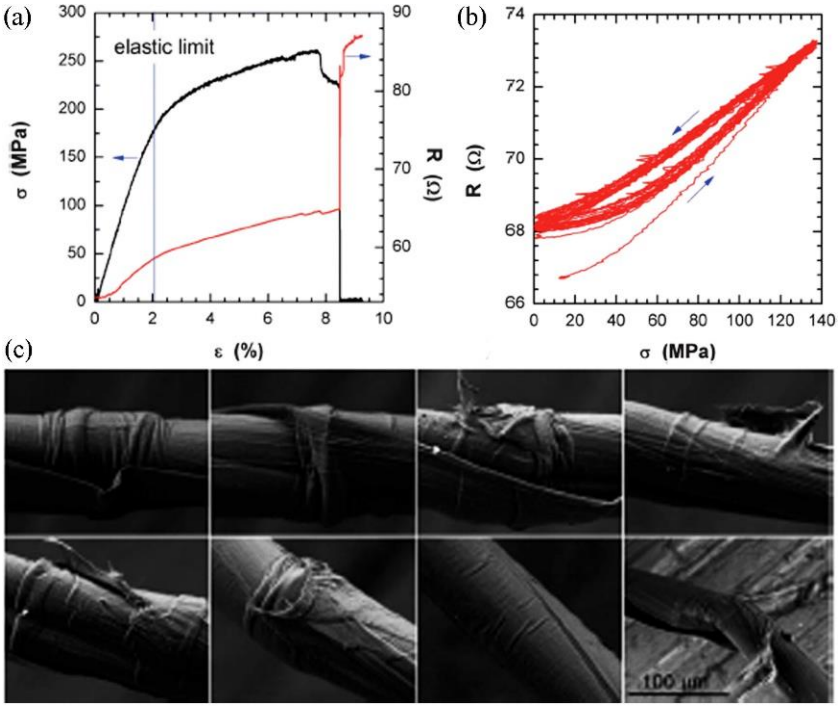

Fig. 1. (a) Typical resistance/stress-strain behavior during monotonic tensile loading. (b) Electrical resistance exhibits hysteresis during cyclic tensile loading to 70% F_{max}. (c) Buckling occurring along the length of a fiber specimen. Images taken in sequence from gage (upper left) to failed end (lower right) [1].

As the fibers undergo tensile strain, radial contact between individual carbon nanotubes may improve; however, the degree of axial nanotube-nanotube contact decreases. This behavior gives rise to increases in electrical resistance. Upon failure of the fiber, electrical resistance increases drastically due to a permanent loss of electrical contact between the carbon nanotubes (Fig. 1a). During quasi-static cyclic tensile loading in the form of an electrical resistance hysteresis loop (Fig. 1b). This loop becomes more pronounced at higher load cycles and indicates that, at the same stress level, electrical resistance of the fiber is higher during unloading than during loading. Fig. 1c shows that a new phenomenon for carbon nanotube fibers is reported-the aerogel-spun fibers are observed to undergo mild to severe kinking due to tensile failure. This kinking is attributed to compressive failure due to recoil from the fiber free ends.

2.2 Interfacial behaviors between CNT fiber and epoxy resin [2]

The tensile properties of continuous carbon nanotube (CNT) fibers spun from a CNT carpet consisting of mainly double- and triple-walled tubes, and their interfacial properties in an epoxy matrix, are investigated by single fiber tensile tests and microdroplet tests, respectively. The average CNT fiber strength, modulus and strain to failure are 1.2 ± 0.3 GPa, 43.3 ± 7.4 GPa and 2.7 ± 0.5%, respectively. A detailed study of strength distribution of CNT fiber has been carried out. Statistical analysis shows that the CNT fiber strength is less scattered than those of

MWCNTs as well as commercial carbon and glass fibers without surface treatment. The effective CNT fiber/epoxy interfacial shear strength is 14.4 MPa. Unlike traditional fiber-reinforced composites, the interfacial shear sliding occurs along the interface between regions with and without resin infiltration in the CNT fiber.

Fig. 2 shows the microdroplet test set-up. The interfacial shear strength between CNT fiber and epoxy resin was calculated according to the following equation, which is based on the assumption of a constant IFSS between the fiber and its surrounding matrix [3]:

$$IFSS = \frac{F_d}{\pi d_f L_e} = \frac{\sigma_d d_f}{4L_e}$$

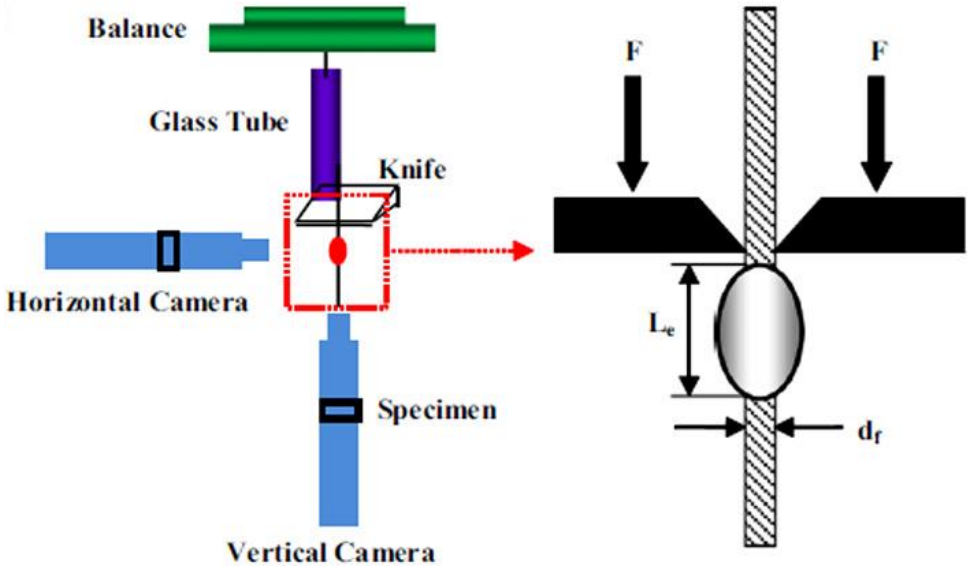

Fig. 2 Microdroplet test set-up [2].

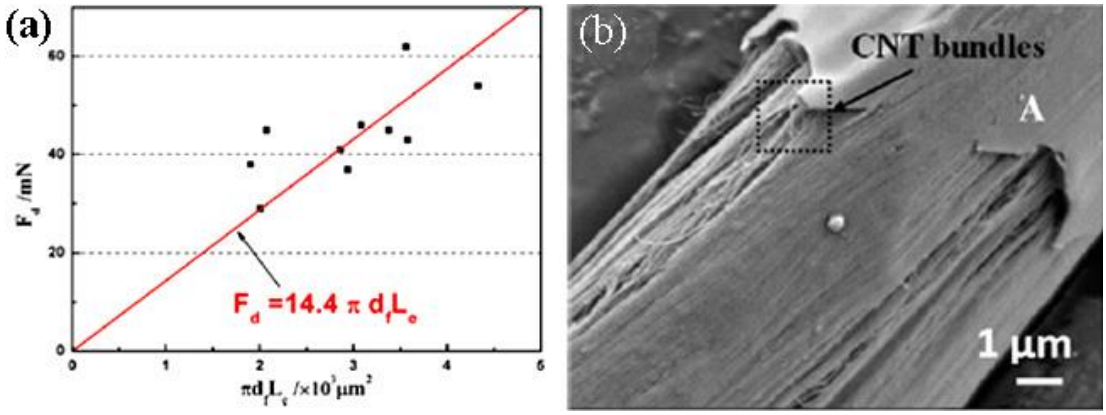

Fig. 3 (a) Debonding force versus embedment area of the microdroplet specimens made of CNT fiber and epoxy. (b) An SEM image of the CNT fiber/epoxy droplet after interfacial debonding [2].

By fitting the experimental data using the least-square method to the linear function passing through the origin (Fig. 3a), the average effective IFSS can be obtained from the slope of the fitting line, which is 14.4 MPa. The CNT fiber/epoxy interfacial shear strength so determined is comparable to those of E-glass/epoxy composite (20 MPa) [4], and carbon fiber/epoxy composite (18.4 MPa) [5]. After interfacial failure, some CNT bundles were pulled out from the epoxy layer, which indicates the infiltration of the resin matrix in the fiber (Fig. 3b). In addition, there is an obvious fracture zone of CNT bundles in the debonding location at the bottom of the droplet and the diameter of the fiber above this zone is smaller than that below the zone.

2.3 Analysis of the entanglements in CNT fibers using a self-folded nanotube model [6]

CNT entanglements always exist in CNT fibers and play a crucial role in affecting their mechanical properties. In this study, the CNT entanglement is modeled as two connecting SFCNTs. At large aspect ratios, a CNT is energetically favorable to be self-folded due to the van der Waals interactions between different parts of the CNT. The geometrical characteristics of the SFCNTs, such as the critical length for self-folding as well as the critical effective width and length, are investigated by using both an exact theoretical model and an approximate theoretical model. The tensile properties of the SFCNTs have been examined by using both the approximate theoretical model and atomistic simulations. Good agreements are achieved in the results of these two approaches.

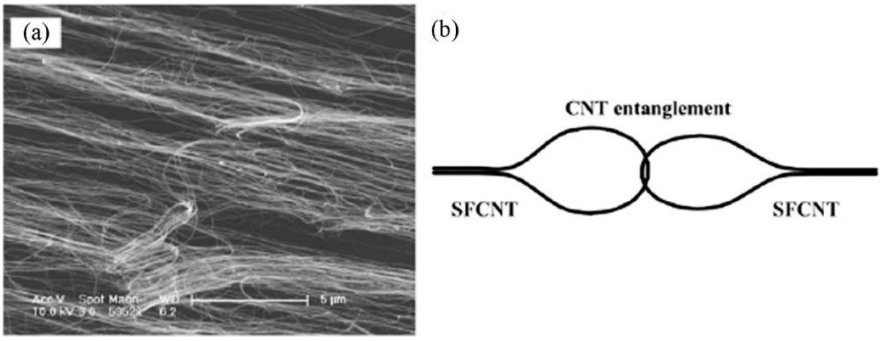

Fig. 4. (a) An SEM image of a freshly drawn CNT fiber [7] and (b) schematic diagram of a CNT entanglement model [6].

CNTs in the fiber are not uniformly aligned and they always tend to entangle with one another, especially in the region connecting two consecutive CNT bundles (Fig. 4a). A simplified model is adopted, where the configuration of CNT entanglement is composed of two SFCNTs, as shown in Fig. 4b. The load that is applied on one side of the entanglement is transferred to the other side through the intersecting point of the two SFCNTs. a long CNT often exists in the self-folded state due to its large aspect ratio and van der Waals interactions between different parts of the CNT. When the two ends of along CNT get closer, they will bind toward each other under the drive of van der Waals interactions and consequently, a racket-like self-folded CNT is formed, as shown in Fig. 4b.

2.4 Review of the state-of-the-art of CNT fibers [8]

The superb mechanical and physical properties of individual carbon nanotubes (CNTs) have provided the impetus for researchers in developing high performance continuous fibers based upon CNTs. The reported high specific strength, specific stiffness and electrical conductivity of CNT fibers demonstrate the potential of their wide application in many fields. In this review paper, we assess the state of the art advances in CNT-based continuous fibers in terms of their fabrication methods, characterization and modeling of mechanical and physical properties, and applications. The opportunities and challenges in CNT fiber research are also discussed.

2.5 Compressive properties of CNT fibers [9, 1]

We recently studied the compressive properties of both pure CNT fibers and epoxy infiltrated CNT fibers using the tensile recoil measurement. The compressive strengths were obtained as 416 and 573 MPa for pure CNT fibers and CNT/epoxy composite fibers, respectively. In addition, microscopic analysis of the fiber surface morphologies revealed that the principal recoil compressive failure mode of pure CNT fiber was kinking, while the CNT/epoxy composite fibers exhibited a failure mode in bending with combined tensile and compressive failure morphologies. CNT fibers tested in this study were spun by drawing and twisting of CNT strips out of vertically well-aligned CNT arrays (forests) [10], whose CNTs were mainly double- and triple-walled with diameters of ~6 nm. CNT/epoxy composite fibers were prepared using a soaking technique [11].

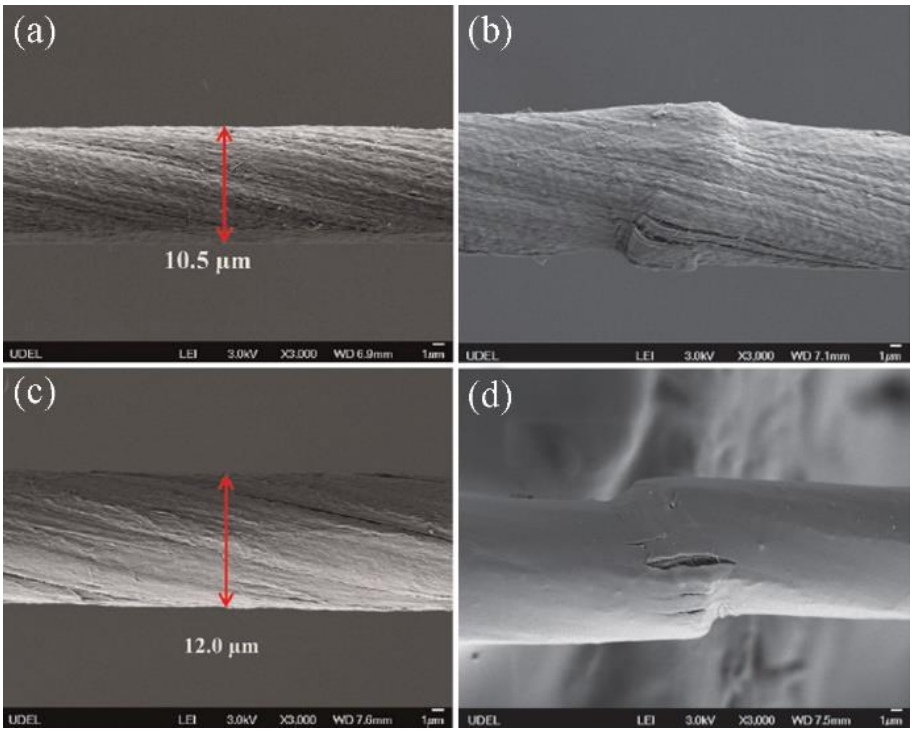

Fig. 5. Surface morphology and compressive damages at locations away from the clamped end for pure CNT fiber (a, b) and CNT/epoxy composite fiber (c, d), respectively [9].

When a pure CNT fiber after recoil test at intermediate initial tensile stress of 680.5 MPa, compressive damage and kinked locations along the upper specimen segment near the clamped end can be easily identified (Fig. 5a, b). The recoil compressive strength of the pure CNT fiber in our study was around 416.2 MPa. For CNT/epoxy composite fibers (Fig. 5c, d), the same method showed the recoil compressive strength is around 573 MPa, which is 37.7% higher than that of the pure CNT fiber. The enhanced compressive strength coupled with the improvement in the tensile strength is due to the effectiveness of resin infiltration.

Tensile strength/MPa	Kink formation
113.5	y
118.2	n
127.4	y
148.3	n
149.2	n
160.1	n
163.2	n
167.7	n
171.3	n
172.1	n
177.2	y
182.6	y
185.9	n
190.1	y
190.3	y
199.6	y
208.2	y
211.0	y
222.2	n
223.3	y
245.9	n
249.6	y
250.9	y
258.5	y

Table 1. Ranked recoil test results [1].

The compressive strength of the aerogel-spun carbon nanotube fibers was estimated by employing the fiber recoil method. By ranking experimental results by strength and observing whether or not kinks formed during tensile failure (Table 1), we find that the majority of fibers tested above 177.2 MPa exhibit kinking while fibers tested below 172.1 MPa generally do not. Therefore, we conclude that compressive strength of the fiber falls in the range of 172–177 MPa.

2.6 Torsional behavior of CNT fibers [12]

Carbon nanotube fibers possess the ability to respond electrically to tensile loading. The electrical response to torsional loading results demonstrate that applied twist compacts the fiber, resulting in increased electrical contact between carbon nanotubes. Shear strains in excess of 24% do not result in permanent changes in electrical resistance along uninfused fibers, while irreversible changes in electrical resistance arise from applied shear strains of 12.9% in epoxy infused fibers. Bulk shear modulus is approximated to be 0.40 ± 0.02 GPa for unreinforced and 2.79 ± 0.64 GPa for infused fibers.

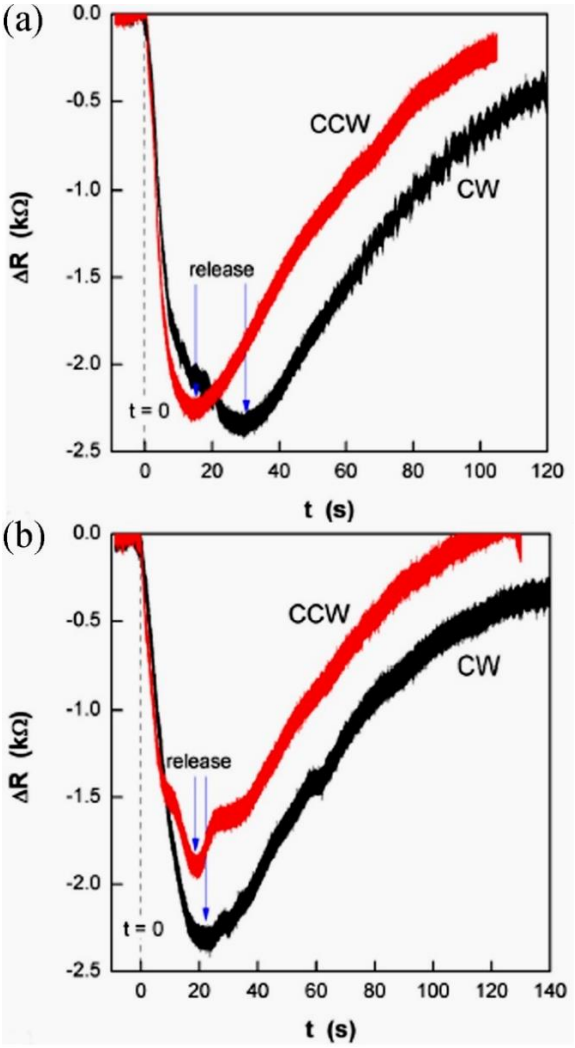

Fig. 6. Changes in electrical resistance arising from CW and CCW twisting in (a) uninfused and (b) infused carbon nanotube fibers. Twisting initiates at t = 0 s [12].

Fiber electrical resistance was measured during the typical torsional experiment, as shown in Fig. 6. From rest, the pendulum is rotated three turns CW or CCW. In each instance, for both uninfused and infused fibers, electrical resistance decreases temporarily upon shear strain application. Once the fiber has returned to its rest state, electrical resistance returns to its baseline value. Note that the electrical resistance decreases further in the case of clockwise rotation. We

attribute this to a residual effect from the applied clockwise twisting during fiber post-processing. To confirm that the electrical resistance recovery is related to fiber untwisting, fibers were twisted and held in place. During this hold period, no electrical resistance recovery occurred.

2.7 Tensile strength relaxation behavior of CNT fibers [13]

To examine the long-term durability of CNT fibers, we studied the time-dependent behavior of CNT fibers, and particularly focused on the tensile stress relaxation. Both the pure CNT fiber and the CNT/epoxy composite fiber exhibited significant stress decay during the relaxation process, and this time-dependent behavior became more significant at a higher initial strain level, a lower strain rate and a greater gauge length. This research provided the fundamental guidance for the long-term durability of CNT fibers in load-bearing multifunctional applications.

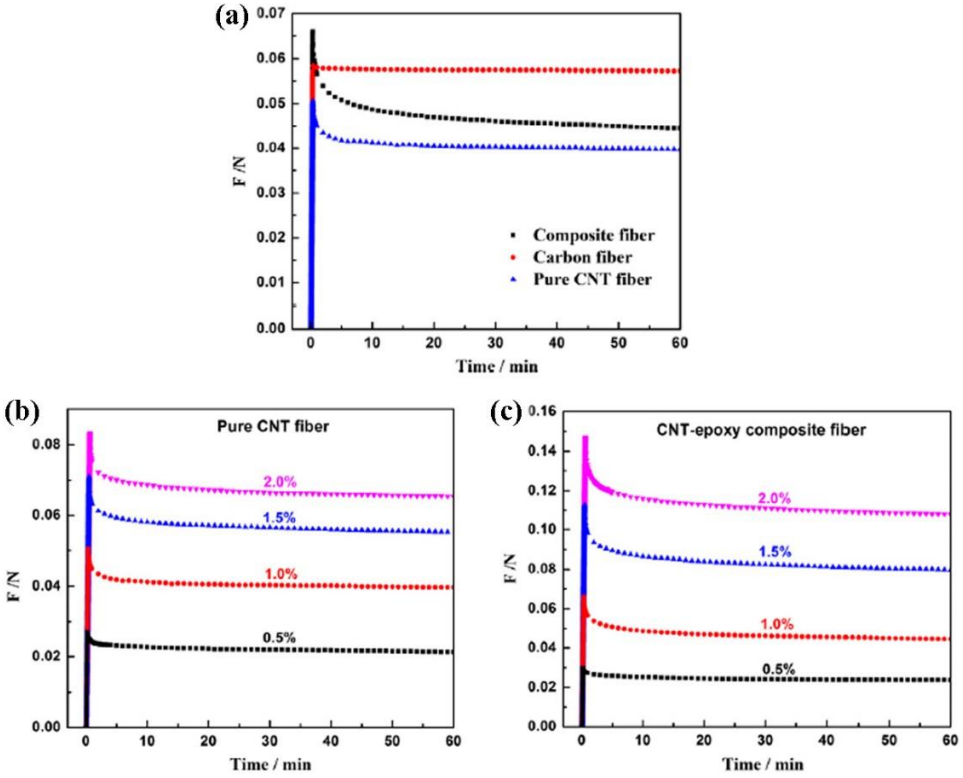

Fig. 7. (a) Force as a function of time during loading and relaxation. Comparisons of relaxation behavior of carbon fiber, pure CNT fiber and CNT/epoxy composite fiber. Effect of initial strain level on the relaxation behavior of CNT fibers. Force as a function of time during the loading and relaxation of (a) pure CNT fiber and (b) CNT/epoxy composite fiber [13].

The tensile stress relaxation behavior of carbon fiber, pure CNT fiber and CNT/epoxy composite fiber were studied for comparison (Fig. 7a). The load of the carbon fiber was almost constant after 1 h and decreased by only 5.4% even after being held for 18 h at the constant initial strain. As for pure CNT fiber, there was significant load decay during the first four minutes of the relaxation process, and the load dropped by as much as 32% after 18 h at constant strain. While

the CNT/epoxy composite fibers showed the highest stress relaxation rate. Fig. 7b and c showed that pure CNT fiber and CNT/epoxy composite fibers have different stress relaxation rate when the initial strains are different.

Initial strain level (%)	E_0–E_∞ (GPa)		τ (s)		E_0 (GPa)		E_∞ (GPa)	
	Pure	Composite	Pure	Composite	Pure	Composite	Pure	Composite
0.5	0.04	0.04	251.6	290.5	0.20	0.19	0.16	0.15
1.0	0.08	0.14	86.7	196.7	0.38	0.43	0.30	0.33
1.5	0.11	0.21	205.5	212.1	0.52	0.72	0.41	0.51
2.0	0.13	0.25	135.4	150.4	0.62	0.95	0.49	0.70

Table 2. Summary of the stretched exponential parameters for both the pure CNT fiber and the composite fiber [13].

The stress relaxation behavior was further simulated using the stretched exponential function [14]:

$$E(t) = (E_0 - E_\infty)e^{-(\frac{t}{\tau})^k} + E_\infty \ (0 < k < 1)$$

And the values of k were found to be about 0.40 for both pure CNT fiber and CNT/epoxy composite fiber at all strain levels. The values of the stress relaxation model parameters are given in the Table 2. For both pure fiber and composite fiber, the initial modulus E_0 simulated by the function was almost the same as the experimental value at each initial strain level.

2.8 Strain rate-dependent tensile properties and dynamic electromechanical behavior of CNT fibers [15]

This investigation into the rate-dependent tensile behavior of carbon nanotube (CNT) fibers provides insight into the role of strain rate and specimen gage length on tensile strength. Chemical vapor produced CNT continuous fibers exhibit significantly higher strengths (3–5 GPa) and moduli (80–200 GPa). During dynamic tension evaluation, real-time electrical measurements provide correlations between high rate deformation/damage mechanical behavior and electrical resistance of the fiber specimens. Furthermore, this first look into the dynamic tensile behavior of CNT fibers demonstrates their potential to serve as sensors in high rate applications.

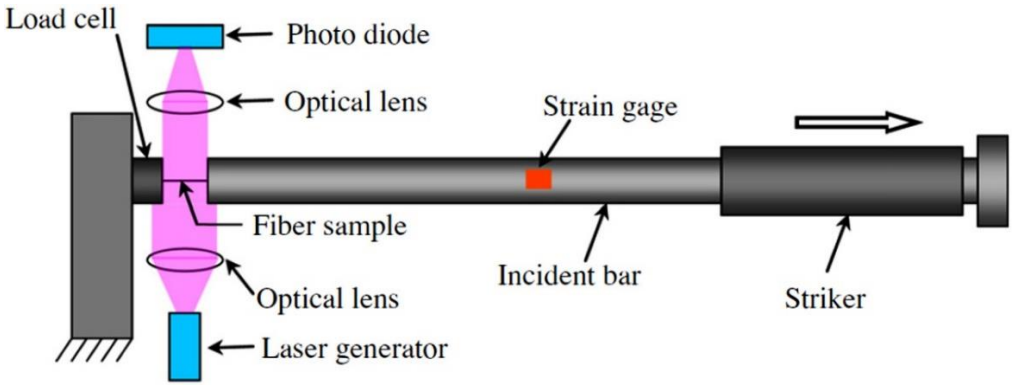

Fig. 8 Kolsky tension apparatus for single fiber evaluation [16].

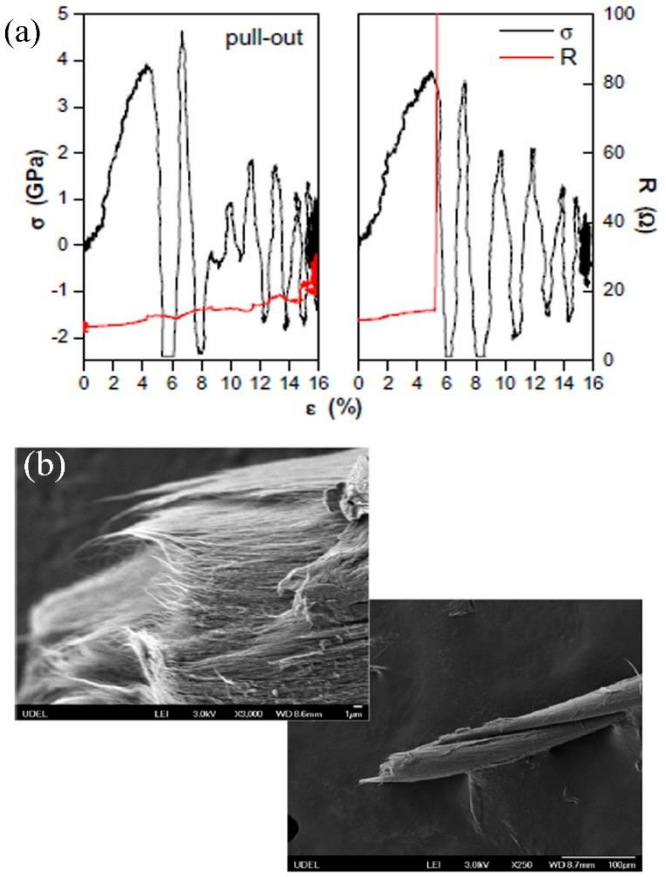

Fig. 9 (a) Electromechanical response to dynamic tension loading for two 3.18 mm gage CNT fiber specimens: pull-out vs. brittle failure. (b) SEM images depicting a CNT fiber failure ends [15].

Fig.8 shows the Kolsky tension apparatus used for CNT fiber test. Fig. 9a shows the electromechanical behavior of two stretched CNT fiber specimens. We present a case of fiber pull-out compared with fiber breakage during loading. In the case of fiber pull-out, electrical resistance increases only slightly due to permanent strain rendering post-examination redundant. The ability to sense strain and damage within a CNT fiber under dynamic tensile loading provides a solid proof of concept for CNT fiber-based sensing in high-rate composite applications. And upon failure (Fig. 9b), electrical resistance becomes infinite due to complete separation of the broken fiber ends.

2.9 CNT fibers based stretchable conductor [17]

By demonstrating the multifunctional properties of CNT fibers, we recently designed a CNT fiber based stretchable conductor by a simple prestraining-then-buckling approach. Before being transferred to the prestrained substrate, CNT fibers were coated with a thin layer of liquid PDMS

by a dip-coating method to enhance interfacial bonding between the fibers and the PDMS substrate and thus, facilitate the buckling formation. Upon curing and releasing of the prestrain, the CNT fibers were kinked laterally. By contrast, the T300 carbon fibers adhered to the prestrained substrate were fractured into segments instead after release of the prestrain due to their high flexural modulus. A stretchable conductor was constructed by further coating the buckled CNT fibers with a thin layer of PDMS (Fig. 10).

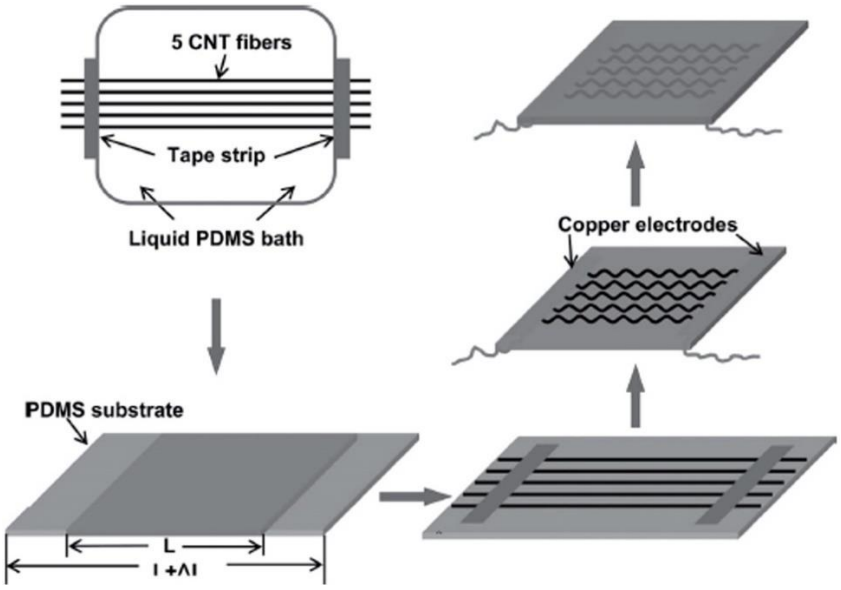

Fig. 10 Illustration of the fabrication process of buckled CNT fibers sandwiched in between PDMS [17].

Massive CNT fiber buckles formed in the stretchable conductor as shown in Fig. 11a, which was generated from the compressive force induced by releasing the fiber/substrate assembly from prestrain. The height of the kinked fiber was in the range of 20–30 μm, much higher than that of the fiber diameter which was around 13 μm. The CNT bundles on the compressive side of the fiber buckled without apparent damage to the fibers. Moreover, the buckled CNT fiber can be alternatively straightened and kinked without apparent permanent fracture under stretching-and-releasing cycles.

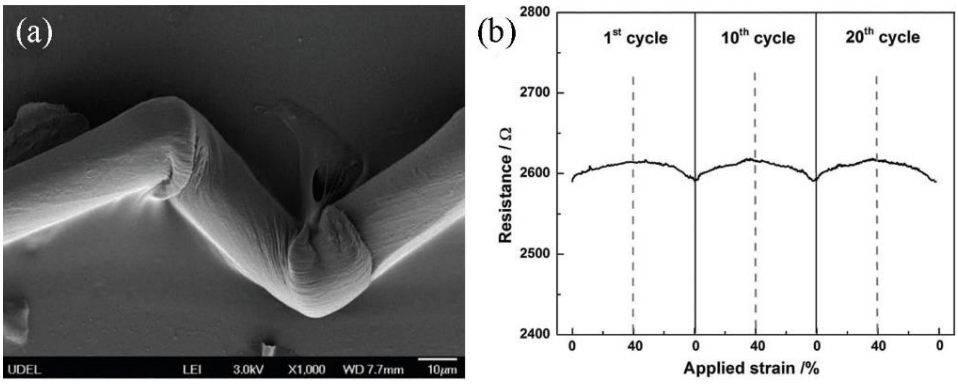

Fig. 11 (a) An SEM image shows two kinks in the CNT fiber. (b) Electrical resistance of a CNT fiber/PDMS composite fi lm during cyclic stretching to the prestrain level of 40%. Only the data of the 1st, 10th, and 20th cycles are shown for comparison [17].

Fig, 11b plots the measured resistance of the CNT fiber/PDMS film during cyclic stretching to the prestrain level of 40%. It can be seen that the resistance of the composite film increased slightly with increasing tensile strain by only about 30 Ω (1%) up to the prestrain level. Upon release, the resistance showed a corresponding decrease, eventually returning to its initial state. This trend of resistance variation was maintained in multiple stretching-and-releasing cycles up to the prestrain level. The excellent stability and repeatability of the kinking of the CNT fibers are of critical importance in retaining the fiber electrical conductivity during cyclic loading, and therefore performance of CNT fiber based stretchable conductors.

2.10 Simulations of mechanical behavior and microstructural evolution of CNT fibers [20, 21]

The tensile behavior of CNT films and fibers were investigated by coarse-grained molecular dynamics (CGMD) simulations, and a comprehensive investigation of the mechanical behavior and microstructural evolution of CNT continuous fibers under twisting and tension was performed. Results indicate that twisting can make either positive or negative contributions to the mechanical properties of the resulting CNT fiber, depending on the microstructure. CNT entanglements always exist in CNT fibers and play a crucial role in affecting their mechanical properties. This study would be helpful not only in the general understanding of the nano- and micro-scale factors affecting CNT fibers' mechanical behavior, but also provide an effective means of revealing the structure/property relationships of CNT films/fibers, which are essential in designing high performance CNT fibers.

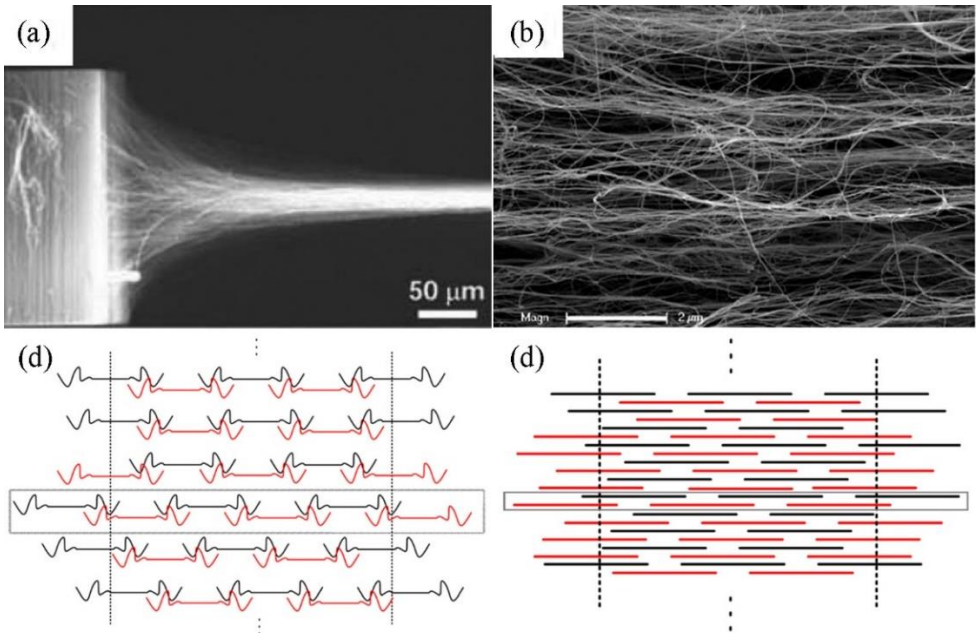

Fig. 12 (a) SEM micrographs showing CNT structures formed during the dry-drawing process [20] and, (b) the as produced CNT films [21]. (c, d) Simulation models for entangled and straight CNT films, respectively [18].

Fig. 12a shows a snapshot during the fiber drawing process, where it is evident that a triangular zone forms the area in which CNTs leave the array. And it clearly illustrate the CNT entanglements found in the obtained CNT film (Fig. 12b). Thus, a new CNT film model with both the entangled and straight CNT structures (Fig. 12c, d) is developed to simulate the structural evolution of CNT films and fibers under tension using the CGMD method.

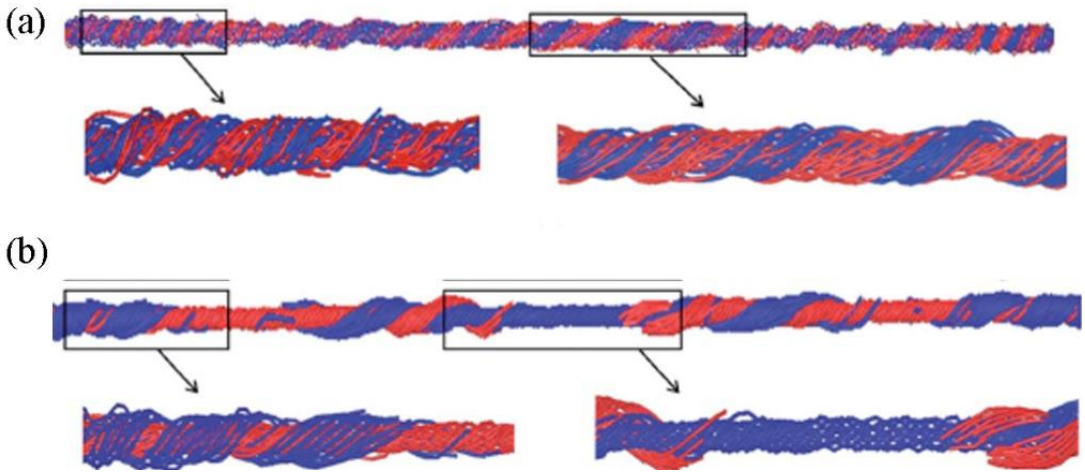

Fig. 13 Structural reorganization of (a) fiber with random CNT stacking and (b) fiber with regular CNT stacking after twisting. Enlarged images show the morphologies at different sections of the fibers. The CNTs in the top and bottom layers of the CNT film are colored in red and blue, respectively [19].

Twisting simulations are carried out to investigate the configurations of CNT fibers twisted from CNT films with random and regular end stacking (Fig. 13). And the simulation results showed that the highest tensile strength is 0.62 GPa and 0.57 GPa for random and regular CNT stacking fibers, respectively. Our CGMD simulation results also demonstrated the twisting process has resulted in different tensile behavior of CNT fibers with entangled CNTs and straight CNTs, and the former is enhanced while the latter is degraded (which are similar to the CNT fibers stacked from random and regular CNTs, respectively). In the simulation work, we established three microstructural evolution mechanisms, namely CNT stretching, fiber untwisting (or unbending of the CNTs) and intertube sliding, have been identified for describing the CNT fiber deformation, and good agreements are achieved with the experimental results.

2.11 A literature review of CNT fibers for advanced composites [22]

Investigations into carbon nanotube fibers as not only structural reinforcement materials but also standalone or embedded strain/damage, thermal, atmospheric and biochemical sensors are driven by their high specific strength, stiffness, electrical and thermal conductivity, and extreme flexibility. With future applications in view, we have studied their load transfer mechanisms, coupled electrical and mechanical response, high strain rate behavior and adaptability to resin infusion. This article is intended to cover our research over the past couple years and to highlight relevant and interesting work performed by others in the area of carbon nanotube fiber mechanics and experimental characterization.

2.12 Interfacial behavior of CNT/graphene hybrid fibers [23]

Highly aligned CNT film wrapped graphene composite fibers was fabricated by directly rolling CNT film around a graphene fiber with the CNTs paralleled to the axial direction of graphene fiber. After wrapping, the specific strength and electrical conductivity of graphene fiber were simultaneously enhanced by 22% and 49% (to 89 mN/tex and 212 S/cm), respectively. Thicker CNT film wrapping of the rGO fiber induces a core-sheath structure; the resulting interfacial debonding and slippage under fiber axial loading were examined.

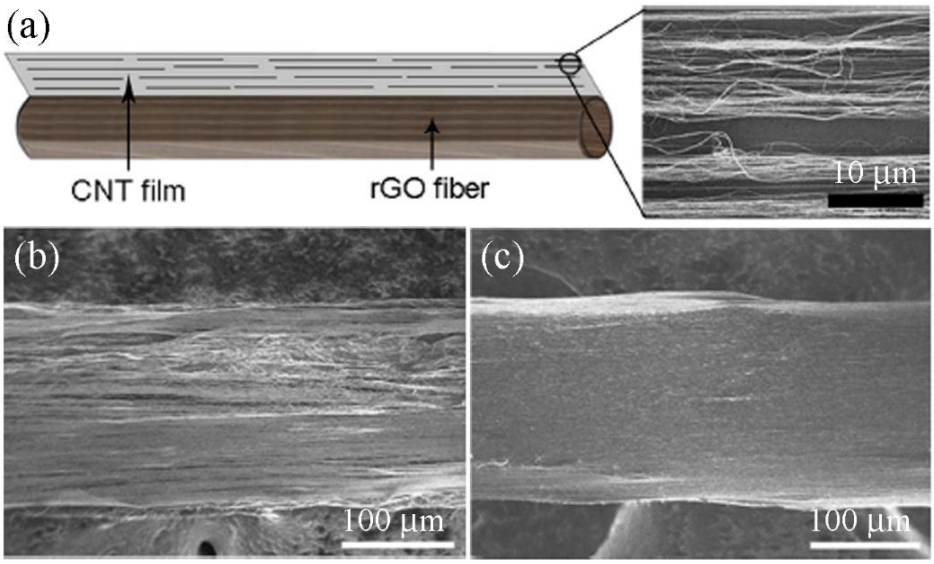

Fig. 14 (a) Schematic illustration of CNT film wrapping a graphene fiber and an SEM image of the aligned CNT film. (b, c) CNT/graphene hybrid fibers with different amounts of CNTs [23].

We wrap the graphene fiber with highly aligned CNT film (Fig. 14a). After the hybrid fibers were densified with ethanol, 1.57 and 9.42 mm width CNT film wrapped fiber show different surface coverage conditions (Fig. 14b, c). The specific strengths of CNT/graphene hybrid fibers were improved compared with the pristine graphene fiber (Fig. 15a). The sudden load drop obviously seen in fiber f3 and f4 was attributed to the sudden debonding and slippage between the CNT film sheath and the graphene fiber core, which resulting in corresponding fiber electrical resistance variation with tensile strain increased (Fig. 15b), and finally led to the core fiber being extracted from the CNT film sheath (Fig. 15c). Combined with the phenomenon that the hybrid fibers' electrical conductivities were also greatly increased, these suggest that the core-sheath fiber structure had a significant influence on the interfacial properties between CNT and graphene in the hybrid fibers.

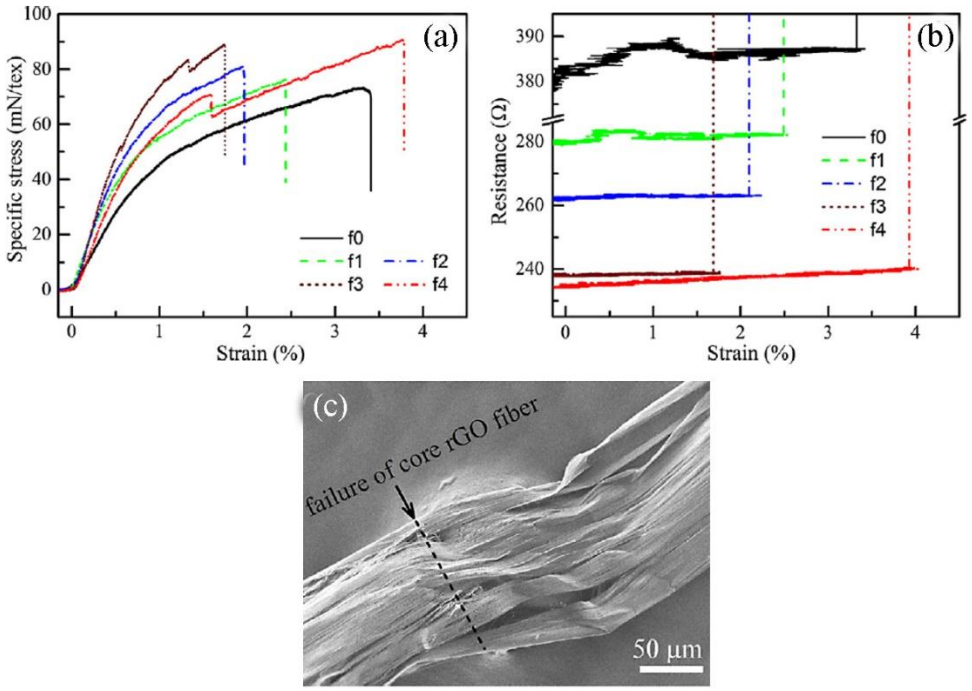

Fig. 15 Specific tensile stress-strain curves (a) and the corresponding electrical resistance-strain curves (b) of graphene fiber (f0) with wrapping CNT film width of 1.57, 3.14, 6.28 and 9.42 mm (f1, f2, f3 and f4, respectively). (c) Failure of the CNT/graphene hybrid fiber [23].

2.13 High performance porous CNT/PVA fibers [24]

We synthesized porous CNT fibers with high mechanical strength and electrical conductivity by a wet spinning method. Commercialized CNT sizing material was used as the precursor, and low concentration (0.1 wt%) PVA/H_2O solutions with the assistance of a small amount of H_2SO_4 (1 wt%) was employed as the coagulation bath.

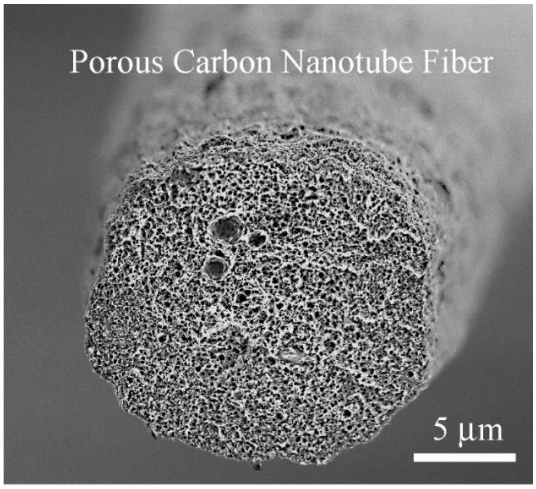

Fig. 16 An SEM image shows the porous structure of the cross section of the porous CNT/PVA fiber [24].

The tensile strengths of the porous CNT/PVA fibers with different contractions of 41%, 30% and 10% are 121, 140 and 231 MPa, respectively. And the electrical conductivity of this porous fiber (Fig. 16) is as high as 1778 S/m, more than 10 times higher than that of CNT fiber spun from 5% PVA solution [25], and even higher than that of pure wet-spun CNT fibers (667 S/m) [26]. This was attributed to the low concentration of insulating PVA used.

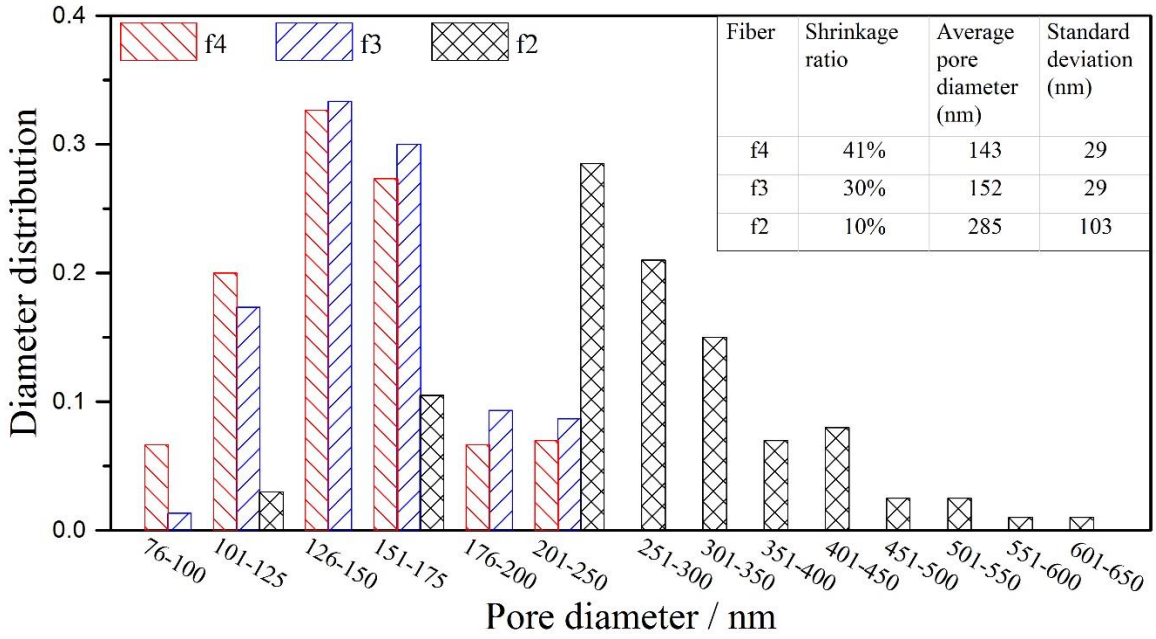

Fiber	Shrinkage ratio	Average pore diameter (nm)	Standard deviation (nm)
f4	41%	143	29
f3	30%	152	29
f2	10%	285	103

Fig. 17 Pore diameter distribution of CNT/PVA fibers with different contractions. The contraction ratio and pore size of each fiber are listed in the top right inset table [24].

Our results showed that 90% of the pore diameters in porous CNT/PVA fiber f2 were in the range of 150–450 nm (average diameter of 285 nm, Fig. 17). The pore diameter is far larger than the mesopores (2–50 nm) that typically existed in dry-spun CNT fiber [27]. By controlling fiber contraction ratio during drying process, fibers with smaller-size pores of 152 and 143 nm were also obtained, with more than 80% of those were in the range of 100–175 nm. CNT fibers with large size pores may have promising applications for accommodating foreign particles to fabricate multifunctional composites fibers [28] and accessing of large polymer chains to enhance fiber mechanical properties [29].

2.14 Electromechanical behavior of reduced graphene fibers [30]

In this study, the electromechanical response of reduced graphene oxide (rGO) fiber is reported. The rGO fiber shows immediate Young's modulus decrease upon electric current application, and the load-drop can be as high as 82% of the original loading when a 20 mA current is applied. Joule heating induced dynamic absorption and desorption of water molecules induced rGO sheet sliding is responsible for this behavior. Electromechanical responses of rGO fibers open the door for future development of functional rGO fiber in the fields of actuators and sensors.

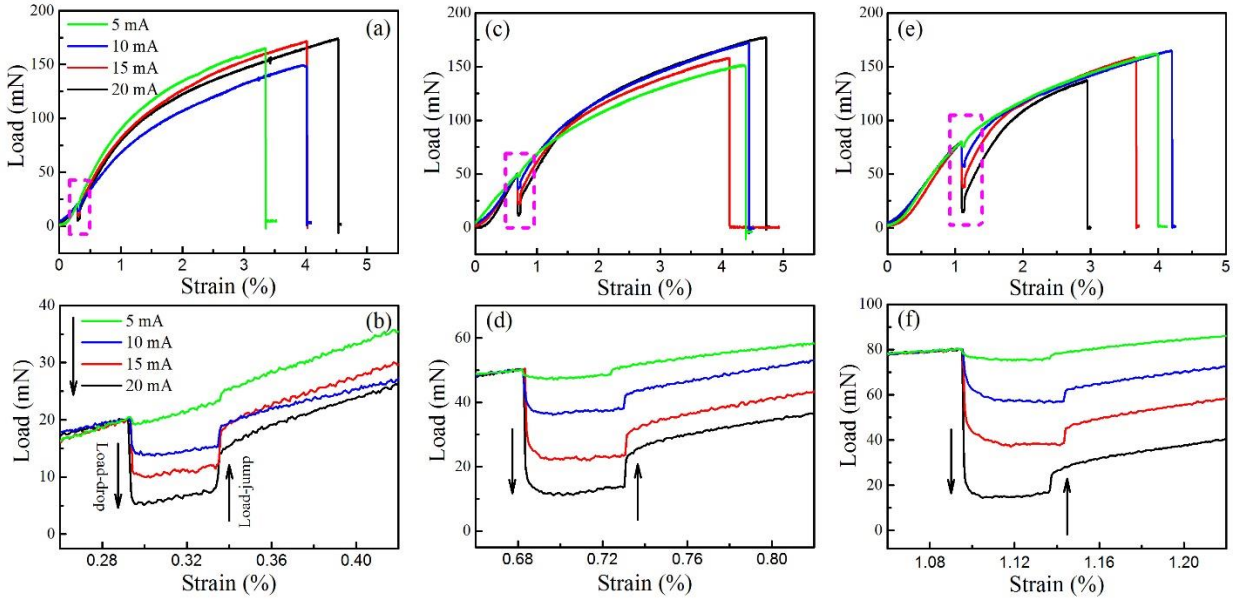

Fig. 18 Mechanical responses of rGO fibers during continuous stretching when different electric currents are applied at the tensile loadings of (a) 20 mN, (c) 50 mN and (e) 80 mN, and the corresponding load-drop/jump curves are enlarged in (b), (d) and (f), respectively [30].

The rGO fiber has an immediate and significant mechanical response when an electric current is applied. As shown in Fig. 18a and b, when currents of 5, 10, 15 and 20 mA were applied at the tensile loading of 20 mN, load-drops of 1.3, 5.8, 9.9 and 14.8 mN emerged immediately. The initial fiber modulus can be calculated by: $E_f = F/\varepsilon A$ (E_f: Young's modulus, F: tensile loading, A: cross-sectional area), and the tensile loading on fiber is given as $\pi E_f \varepsilon d^2/4$. At the end of 5 s current application, immediate load-jumps were observed (Fig. 18b). During this process, the rGO fibers' moduli further increased by 0.36 (5 mA), 1.12 (10 mA), 1.78 (15 mA) and 2.24 GPa (20 mA), respectively. Fig. 18c, d and e, f demonstrate more remarkable mechanical responses when the current was applied at higher tensile loadings of 50 and 80 mN.

2.15 A literature review of graphene-based fibers [31]

Significant progress has been made in recent years in the development of graphene-based fibers (GBFs) due to their unique structures and excellent properties. Potential applications of GBFs can be found, for instance, in stretchable conductors, energy storage and conversion devices, actuators, field emitters, solid-phase microextraction and catalysis. Different from graphene-based aerogels (GBAs) and membranes (GBMs), GBFs have demonstrated remarkable mechanical and electrical properties, and can be bent, knotted, or woven into flexible electronic textiles. Therefore, it is timely that a comprehensive assessment of the state-of-the-art in GBF research and development be made. To this end, we have conducted an extensive literature review of GBFs with focus on their synthesis, performance and application. We also attempt to identify the future directions in GBF research.

3. Summary

Continuous carbon nanotube fibers possess high mechanical properties and electrical conductivity, demonstrating the potential of multifunctional applications in various fields. In this program, we systematically studied the tensile strength, compressive strength, microstructure, torsional behavior, electromechanical response, failure behavior, tensile stress relaxation behavior of CNT fibers, and its interfacial behavior with graphene and polymer materials. We have also investigated the synthesis and electromechanical behavior of GBFs. Molecular dynamic simulations studying the relationship between CNT assemblies and the resulting mechanical and electrical properties were conducted to gain insight into the fundamental strengthening mechanisms. Transparent, stretchable composites based on CNT fibers and PDMS were also designed and fabricated to demonstrate the multifunctional applications of CNT fiber. Eleven journal papers and two review articles summarizing the research progress and future development have been published; two journal papers and one review article are under preparation.

References:

1. A. S. Wu, T. -W. Chou, J. W. Gillespie, Jr., D. Lashmore and J. Rioux. Electromechanical response and failure behaviour of aerogel-spun carbon nanotube fibres under tensile loading, *Journal of Materials Chemistry*, **22**, 6792–6798, 2012.

2. M. Zu, Q. W. Li, Y. T. Zhu, M. Dey, G. J. Wang, W. B. Lu, J. M. Deitzel, J. W. Gillespie Jr., J. -H. Byun and T. -W. Chou. The effective interfacial shear strength of carbon nanotube fibers in an epoxy matrix characterized by a microdroplet test, *Carbon*, **50**, 1271–1279, 2012.

3. B. Miller, P. Muri and L. Rebenfeld. A microbond method for determination of the shear-strength of a fiber-resin interface, *Composites Science and Technology*, **28**, 17–32, 1987.

4. N. Netravali, D Stone, S Ruoff and L. T. T. Topoleski. Continuous micro-indenter push-through technique for measuring interfacial shear-strength of fiber composites, *Composites Science and Technology*, **34**, 289–303, 1989.

5. F. H. Zhang, R. G. Wang, X. D. He, C. Wang and L. N. Ren. Interfacial shearing strength and reinforcing mechanisms of an epoxy composite reinforced using a carbon nanotube/carbon fiber hybrid, *Journal of Materials Science*, **44**, 3574–3577, 2009.

6. W. B. Lu and T. -W. Chou. Analysis of the entanglements in carbon nanotube fibers using a self-folded nanotube model, *Journal of the Mechanics and Physics of Solids*, **59**, 511–524, 2011.

7. X. B. Zhang, K. L. Jiang, C. Feng, P. Liu, L. N. Zhang, J. Kong, T. H. Zhang, Q. Q. Li and S. S. Fan. Spinning and processing continuous yarns from 4-inch wafer scale super-aligned carbon nanotube arrays, *Advanced Materials*, **18**, 1505–1510, 2006.

8. W. B. Lu, M. Zu, J. -H. Byun, B. -S. Kim and T. -W. Chou. State of the art of carbon nanotube fibers: Opportunities and challenges, *Advanced Materials*, **24**, 1805–1833, 2012.

9. M. Zu, W. B. Lu, Q. W. Li, Y. T. Zhu, G. J. Wang and T. -W. Chou. Characterization of carbon nanotube fiber compressive properties using tensile recoil measurement, *ACS Nano*, **6**, 4288–4297, 2012.

10. J. J Jia, J. N Zhao, G. Xu, J. T. Di, Z. Z. Yong, Y. Y. Tao, C. Fang, Z. G. Zhang, X. H. Zhang, L. X. Zheng and Q. W. Li. A comparison of the mechanical properties of fibers spun from different carbon nanotubes, *Carbon*, **49**, 1333–1339, 2011.

11. E. Bogdanovich and P. D. Bradford. Carbon nanotube yarn and 3-D braid composites. Part I: Tensile testing and mechanical properties analysis, *Composites, Part A*, **41**, 230–237, 2010.

12. A. S. Wu, X. Nie, M. C. Hudspeth, W. W. Chen, T. -W. Chou, D. S. Lashmore, M. W. Schauer, E. Towle and J. Rioux. Carbon nanotube fibers as torsion sensors, *Applied Physics Letter*, **100**, 201908, 2012.

13. M. Zu, Q. W. Li, Y. T. Zhu, Y. Zhu, G. J. Wang, J. -H. Byun and T. -W. Chou. Stress relaxation in carbon nanotube-based fibers for load-bearing applications, *Carbon*, **52**, 347–355, 2012.

14. G. Williams and D. C. Watts. Non-symmetrical dielectric relaxation behaviour arising from a simple empirical decay function, *Transactions of the Faraday Society*, **66**, 80–85, 1970.

15. A. S. Wu, X. Nie, M. C. Hudspeth, W. W. Chen, T. -W. Chou, D. S. Lashmore, M. W. Schauer, E. Tolle and J. Rioux. Strain rate-dependent tensile properties and dynamic electromechanical response of carbon nanotube fibers, *Carbon*, **50**, 3876–3881, 2012.

16. J. Lim, W. Chen, and J. Zheng. Dynamic small strain measurements of Kevlar 129 single fibers with a miniaturized tension Kolsky bar. *Polymer Testing*, **29**, 701–705, 2010.

17. M. Zu, Q. W. Li, G. J. Wang, J. -H. Byun and T. -W. Chou. Carbon nanotube fiber based stretchable conductor, *Advanced Functional Materials*, **23**, 789–793, 2013.

18. W. B. Lu, X. Liu, Q. W. Li, J. -H. Byun and T. -W. Chou. Mechanical behavior and structural evolution of carbon nanotube films and fibers under tension: A coarse-grained molecular dynamics study, *Journal of Applied Mechanics*, **80**, 051015, 2013.

19. X. Liu, W. B. Lu, O. M. Ayala, L.P. Wang, A. M. Karlsson, Q. S. Yang and T. -W. Chou. Microstructural evolution of carbon nanotube fibers: deformation and strength mechanism, *Nanoscale*, **5**, 2002–2008, 2013.

20. M. Zhang, S. L. Fang, A. A. Zakhidov, S. B. Lee, A. E. Aliev, C. D. Williams, K. R. Atkinson, and R. H. Baughman, Strong, transparent, multifunctional, carbon nanotube sheets, *Science*, **309**, 1215–1219, 2005.

21. M. H. Miao, J. McDonnell, L. Vuckovic, and S. C. Hawkins, Poisson's ratio and porosity of carbon nanotube dry-spun yarns, *Carbon*, **48**, 2802–2811, 2010.

22. A. S. Wu and T. -W. Chou. Carbon nanotube fibers for advanced composites, *Materials Today*, **15**, 302–310, 2012.

23. F. C. Meng, R. Li, Q. W. Li, W. B. Lu and T. -W. Chou. Synthesis and failure behavior of super-aligned carbon nanotube film wrapped graphene fibers, *Carbon*, **72**, 250– 256, 2014.

24. F. C. Meng, W. B. Lu, Q. W. Li, M. Claes, N. Kchit and T. -W. Chou. Porous carbon nanotube fibers spun from a sizing material, submitted.

25. A. Pénicaud, L. Valat, A. Derr, P. Poulin, C. Zakri, O. Roubeau, M. Maugey, P. Miaudet, E. Anglaret, P. Petit, A. Loiseau and S. Enouz. Mild dissolution of carbon nanotubes: Composite carbon nanotube fibres from polyelectrolyte solutions, *Composites Science and Technology*, **67**, 795–797, 2007.

26. J. Steinmetz, M. Glerup, M. Paillet, P. Bernier and M. Holzinger. Production of pure nanotube fibers using a modified wet-spinning method, *Carbon*, **43**, 2397–2400, 2005.

27. C. Choi, J. A. Lee, A. Y. Choi, Y. T. Kim, X. Lepr, M. D. Lima, R. H. Baughman and S. J. Kim. Flexible supercapacitor made of carbon nanotube yarn with internal pores, *Advanced Materials*, **26**, 2059–2065, 2014.

28. M. D. Lima, S. Fang, X. Lepr, C. Lewis, R. Ovalle-Robles, J. Carretero-Gonzlez, E. Castillo-Martnez, M. E. Kozlov, J. Oh, N. Rawat, C. S. Haines, M. H. Haque, V. Aare, S. Stoughton,

A. A. Zakhidov and R. H. Baughman. Biscrolling nanotube sheets and functional guests into yarns, *Science*, **331**, 51–55, 2011.

29. Y. T. Ye, X. H. Zhang, F. C. Meng, J. N. Zhao and Q. W. Li. Enhancing interfacial adhesion and functionality of carbon nanotube fibers with depolymerized chitosan, *Journal of Materials Chemistry C*, **1**, 2009–2013, 2013.
30. F. C. Meng, M. Wang, W. B. Lu, Q. W. Li, T. -W. Chou. Electromechanical behavior of reduced graphene oxide fiber, in preparation.
31. F. C. Meng, W. B. Lu, Q. W. Li, J. -H. Byun, B. -S. Kim, T. -W. Chou. Graphene-based fibers: A review, in preparation.

Personnel Supported:

Tsu-Wei Chou, Principal Investigator

Weibang Lu, Research Associate

Amanda Wu, Research Associate

Fancheng Meng, Research Associate

Mei Zu, Graduate student

Journal Publications of the PI's Research Group During the Grant Period:

1. W. B. Lu and T. -W. Chou. Analysis of the entanglements in carbon nanotube fibers using a self-folded nanotube model, *Journal of the Mechanics and Physics of Solids*, **59**, 511–524, 2011.
2. M. Zu, Q. W. Li, Y. T. Zhu, M. Dey, G. J. Wang, W. B. Lu, J. M. Deitzel, J. W. Gillespie Jr., J. -H. Byun and T. -W. Chou. The effective interfacial shear strength of carbon nanotube fibers in an epoxy matrix characterized by a microdroplet test, *Carbon*, **50**, 1271–1279, 2012.
3. W. B. Lu, M. Zu, J. -H. Byun, B. -S. Kim and T. -W. Chou. State of the art of carbon nanotube fibers: Opportunities and challenges, *Advanced Materials*, **24**, 1805–1833, 2012.
4. A. S. Wu, T. -W. Chou, J. W. Gillespie Jr., D. Lashmore and J. Rioux, Electromechanical response and failure behavior of aerogel-spun carbon nanotube fibers under tensile loading, *Journal of Material Chemistry*, **22**, 6792–6798, 2012.
5. A. S. Wu, X, Nie, M. C. Hudspeth, W. W Chen, T. -W. Chou, D. Lashmore, M. Schauer, E. Tolle and J. Rioux. Strain rate-dependent tensile properties and dynamic electromechanical response of carbon nanotube fibers, *Carbon*, **50**, 3876–3881, 2012.

6. M. Zu, W. B. Lu, Q. W. Li, Y. T. Zhu and T. -W. Chou. Characterization of carbon nanotube fiber compressive properties using tensile recoil measurement, *ACS Nano*, **60**, 4288–4297, 2012.
7. A. S. Wu, X. Nie, M. C. Hudspeth, W. W. Chen, T. -W. Chou, D. S. Lashmore, M. W. Schauer, Erick Towel and J. Rioux. Carbon nanotube fibers as torsion sensors, *Applied Physics Letters*, **100**, 201908, 2012.
8. A. S. Wu and T. -W. Chou. Carbon nanotube fibers for advanced composites, *Materials Today*, **15**, 302–310, 2012.
9. M. Zu, Q. W. Li, Y. T. Zhu, Y. Zhu, G. J. Wang, J. -H. Byun and T. -W. Chou. Stress relaxation in carbon nanotube-based fibers for load-bearing applications, *Carbon*, **52**, 347–355, 2013.
10. M. Zu, Q.W. Li, G.J. Wang, J. -H. Byun and T. -W. Chou. Carbon nanotube fiber based stretchable conductor, *Advanced Functional Materials*, **23**, 789–793, 2013.
11. X. Liu, W. B. Lu, O. M. Ayala, L. P. Wang, A. M. Karlsson, Q. S. Yang and T. -W. Chou. Microstructural evolution of carbon nanotube fibers: deformation and strength mechanism, *Nanoscale*, **5**, 2002–2008, 2013.
12. W. B. Lu, X. Liu, Q. W. Li, and J. -H. Byun and T. -W. Chou. Mechanical behavior and structural evolution of carbon nanotube films and fibers under tension: a coarse-grained molecular dynamics study, *Journal of Applied Mechanics*, **80**, 051015, 2013.
13. F. C. Meng, R. Li, Q. W. Li, W. B. Lu and T. -W. Chou. Synthesis and failure behavior of super-aligned carbon nanotube film wrapped graphene fibers, *Carbon*, **72**, 250–256, 2014.
14. F. C. Meng, W. B Lu, Q. W Li, M. Claes, N. Kchit and T. -W. Chou. Porous carbon nanotube fibers spun from a sizing material, submitted.
15. F. C. Meng, M. Wang, W. B. Lu, Q. W. Li, T. -W. Chou. Electromechanical behavior of reduced graphene oxide fiber, in preparation.
16. F. C. Meng, W. B. Lu, Q. W. Li, J. -H. Byun, B. -S. Kim, T. -W. Chou. Graphene-based fibers: A review, in preparation.

Honors/Awards (T. -W. Chou):

2011 Named among top 100 materials scientists of the decade (2000-2010) by Times Higher Education (ranked 34th)
2011 World Fellow, International Committee on Composite Materials
2013 Advisory Professor, Tongji University, Shanghai, China
2013 Nadai Medal, ASME
2014 ASC/DEStech Award in Composites, American Society for Composites

Prior to Current Grant Period (T. -W. Chou):

1994 Honorary Research Professor, Beijing University of Aeronautics & Astronautics, China
1996 Charles Russ Richards Memorial Award, American Society of Mechanical Engineers
1997 Honorary Research Professor, Northwestern Polytechnical University, China
1998 Distinguished Research Award, American Society for Composites
1998 Fellow, American Society of Mechanical Engineers
1999 Fellow, ASM International
2001 Fellow, American Society for Composites
2001 Francis Alison Medal, University of Delaware
2002 Fellow, American Ceramic Society
2002 Highly Cited Researchers, ISI
2002 Worcester Reed Warner Medal, ASME
2003- Pierre S. du Pont Chair of Engineering
2005 Fellow, American Institute of Aeronautics and Astronautics
2008 Fellow, the Mineral, Metals and Materials Society (TMS)
2009 Medal of Excellence in Composite Materials, University of Delaware Center for Composite Materials

Part II: Report by the Co-Principal Investigator

1. Introduction

The following research and support for PI's research have been conducted during the grant period:

Year 1:

Synthesis of spinnable carbon nanotube (CNT) arrays, and fabrication of CNT fibers for supporting the PI's fundamental research of CNT fibers. Multi-walled carbon nanotubes with high level of spinnability and quality have been synthesized. An automated winding and twisting machine has been designed and built for fabricating continuous CNT fibers with required diameter, twist angle, and length. See section 2.1.

- Spun CNT fibers for the electromechanical response and failure behavior of pure CNT fibers and CNT composite fibers under tensile loading. See **Part I** section 2.1 [1]

- Spun CNT fibers for the interfacial behavior of CNT fiber/epoxy composites characterizations. See **Part I** section 2.2 [2]

Year 2:

(1) Synthesis of spinnable CNT arrays, and fabrication of CNT fibers for supporting the PI's fundamental research of CNT fibers. See section 2.1.

(2) Fabrication and examination of mechanical properties and electromechanical properties of CNT fiber composites. CNT fiber composites showed similar mechanical properties to the neat matrix. CNT fiber composites were also tested under cyclic tensile loading to assess their piezoresistive response. No permanent damage was incurred up to 66% of ultimate strength. See section 2.2.

(3) Invention and development of low twist CNT yarns for high performance textiles and composites. This invention provides an assembly of solutions to current problems in CNT fiber fabrication. We obtained very low or zero twist in a CNT fiber (<15°). This invention improves the productivity of CNT fibers, ensures better polymer infiltration, allows stretching of the CNT fibers, and enhances their properties. See section 2.3. [5]

Year 3:

(1) Synthesis of spinnable CNT arrays, and fabrication of CNT fibers for supporting the the PI's fundamental research of CNT fibers. See section 2.1.

(2) Design and development of multi-functional glass fiber reinforced composites (GFRP) with embedded flexible twisted CNT fibers for in-situ strain sensing applications. The embedded CNT fibers demonstrated effective sensing capability when the GFRP was loaded up to 80% of maximum strain. Up to a maximum strain amplitude of 20% of the composite, the strain-

dependent resistance of the CNT fiber showed good recoverability and reproducibility. See section 2.4. [4]

(3) Examination of bending fatigue properties of glass fiber reinforced composites with embedded flexible twisted CNT fibers. The CNT fiber has sensing capability up to 60% of the maximum load, and showed repeatable resistance response when cycled 1000 times at 45% of the maximum load, which is superior to conventional CNT fibers fabricated with dispersed CNTs. See section 2.5. [4]

(4) Plasma-treatment study of raw CNT ribbons that are used to fabricate CNT fibers. Oxygen plasma treatment was found effective to improve the interfacial properties of spinnable CNTs and thus improved the tensile strength of the CNT/Bismaleimide composites by 82%, and Young's modulus by 26%. See section 2.6.

2. Brief Overview of Accomplishments

During the three-year collaborative project, synthesis of spinnable carbon nanotube arrays with high level of spinnability and consistent quality has been achieved. CNT fibers with required diameter, twist angle, length have been designed and fabricated to support the PI's fundamental research. The properties of both raw CNT sheet material and resulting CNT fibers were enhanced by applying unique treatment method and developing novel fabrication technology. Various flexible macroscopic CNT fiber composites have been designed and characterized. Flexible and multi-functional glass fiber composites with embedded CNT fiber are demonstrated promising for the next generation *in-situ* strain and damage sensing as smart structures. The contents are summarized below.

Key Words: Carbon nanotubes, Synthesis, CNT fiber, Composites, Mechanical Properties, Strain Sensing

2.1 Synthesis of spinnable CNT arrays and fabrication of CNT fibers

The CNTs synthesized by the iron chloride ($FeCl_2$) catalyzed growth have multiwalls. Multi-walled carbon nanotubes are more robust for surface treatment, such as doping, compared to single-walled or double-walled nanotubes. Due to the nature of the nucleation of the catalyst nanoparticles in the vapor phase, the catalyst nanoparticle formation is dependent on the partial pressure of the catalyst vapor in the reactor. This partial pressure can be influenced by both the starting amount of catalyst in the reactor and its dilution by reactive or non-reactive gas. We completed experiments to determine the effect of the catalyst starting weight, nucleation temperature, acetylene and argon flow rate on the CNT diameter (by transmission electron microscopy evaluation), drawability (speed at which continuous sheets can be pulled), and quality (Raman G/D ratio).

Most CNT array processing routes involve the deposition of metal catalyst particles using a physical vapor deposition route such as sputtering or evaporation. This is a time consuming step due to pre-deposition pumping and the substrate size being limited to the size of the deposition system. The method adopted by NCSU is based on evaporation of a metal salt catalyst initially reported by Prof. Yoku Inoue [6]. Due to the vapor phase deposition of the catalyst particles at the beginning of the CVD process, CNTs are nucleated on any flat quartz surface in the furnace hot zone. It is a low-pressure nucleation and growth process running at around 5 torr, which allows us to grow uniform arrays on large size substrates without causing diffusion limited uneven growth seen in atmospheric CVD processes. NCSU is currently investigating larger CVD systems and scale up opportunities for this synthesis process (4''- 12'' wide substrates for synthesizing large arrays).

Based on the successful synthesis of spinnable CNT arrays (Figure 1), various CNT fibers with desired diameter, twist angle and length have been fabricated. An automated winding and twisting machine has been designed and built to fabricate CNT fibers (Figure 2).

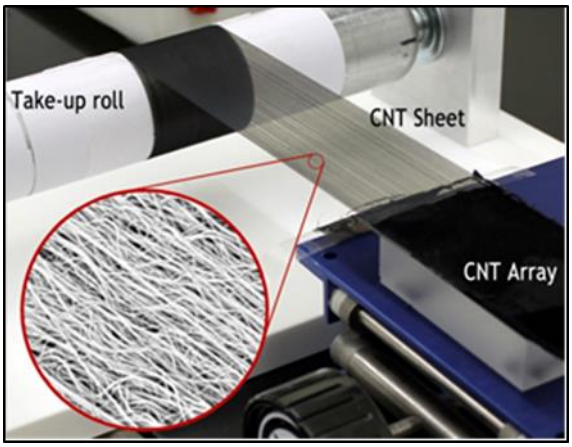

Figure 1. Two inch wide aligned CNT sheet being pulled from a vertically aligned CNT array.

Figure 2. Automated winding and twisting machine designed for fabricating CNT fibers.

2.2 Fabrication and examination of mechanical properties and electromechanical properties of CNT fiber composites.

2.2.1 NCSU hand-woven CNT fiber preforms: Infusion process

The following procedure was used to infuse plain-woven CNT fiber preform (Figures 3-5).

- Acetone treatment and air-drying (30 minutes)
- Nitric acid treatment and oven drying (1 hour at 100ºC)
- Removal from paper holder and placement on a glass substrate cleaned with methanol and treated with Frekote (to aid de-molding).
- Mixing and degassing of the EPON 862:Epikure W (100:26.4) mixture (degassing occurs under vacuum at RT for 30 minutes)
- Pouring of epoxy mixture onto the fiber preform/glass substrate (standard VARTM tape used to prevent overflow)
- Degassing of the preform (under vacuum at 50ºC for 2.5 hours)
- Curing at 130ºC for 6 hours

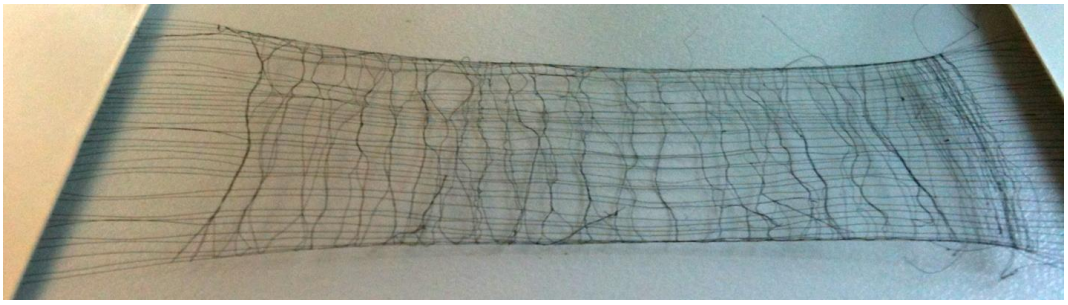

Figure 3. The 90º fibers bunch together via capillary action upon acetone and nitric acid treatment.

Preform Images

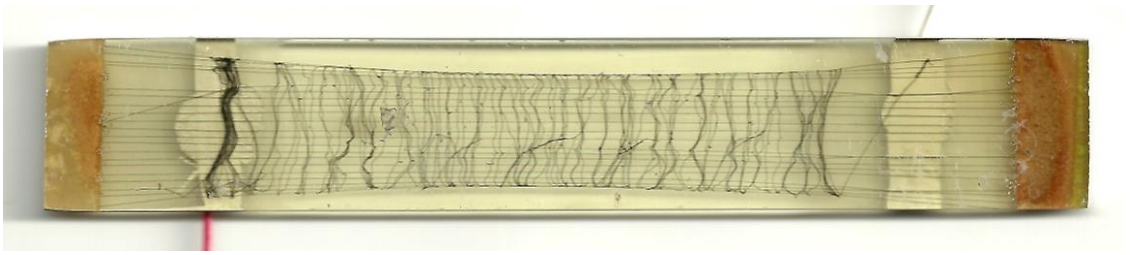

Figure 4. preform prior to end-tabbing

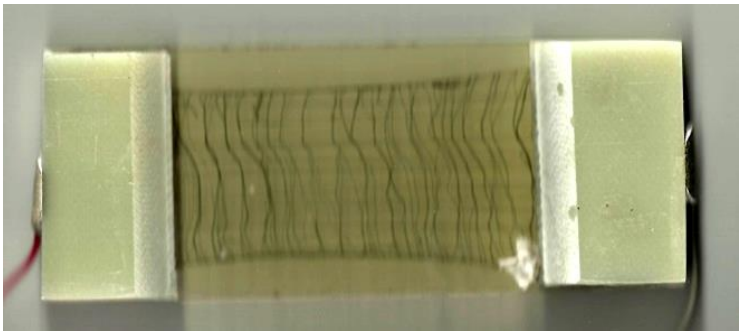

Figure 5. preform with end-tabs and electrodes

2.2.2 Mechanical characterization

Tested specimens 3-6 to failure via ASTM D638 (1.27 mm/min or 0.05 in/min); as expected, strength is ~80 MPa (Figure 6).

In Figure 7, the concept was to evaluate the CNT fiber composites under cyclic tensile loading to assess their electromechancial response. First, a neat epoxy specimen was loaded under incremental cyclic tension to ensure that no permanent damage was incurred up to 66% of maximum tensile strength. Similar results have been found when tested in the PI's group [3].

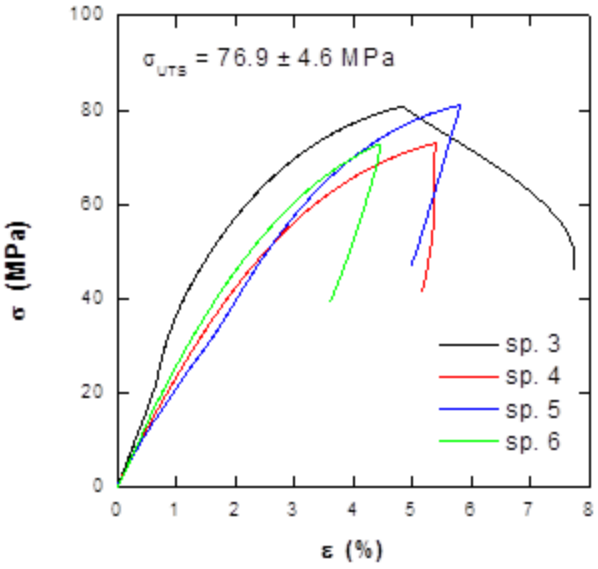

Figure 6. Mechanical behavior of the neat epoxy specimens under monotonic tensile loading

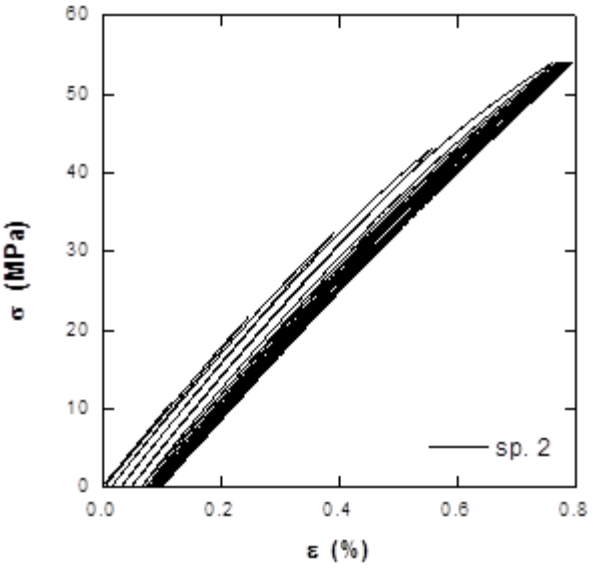

Figure 7. Mechanical behavior of a neat epoxy specimen loaded in 500 N increments to 2500 N (66% σ_{UTS}) and cycled ten times between 0 N and 2500 N.

2.2.3 Electromechanical behavior under bending

Although it is not possible to correlate applied tensile strain directly with electrical resistance changes due to the 90º fibers, we hypothesized that it may be possible to do so under applied three point bending load. To test this hypothesis, the sample was flexed in both directions such that the CNT fiber layer (near the bottom surface of the specimen since it was taped to the mold) was loaded under tension then under compression. We observed a clear increase in electrical resistance measured across the specimen axis (Figure 8).

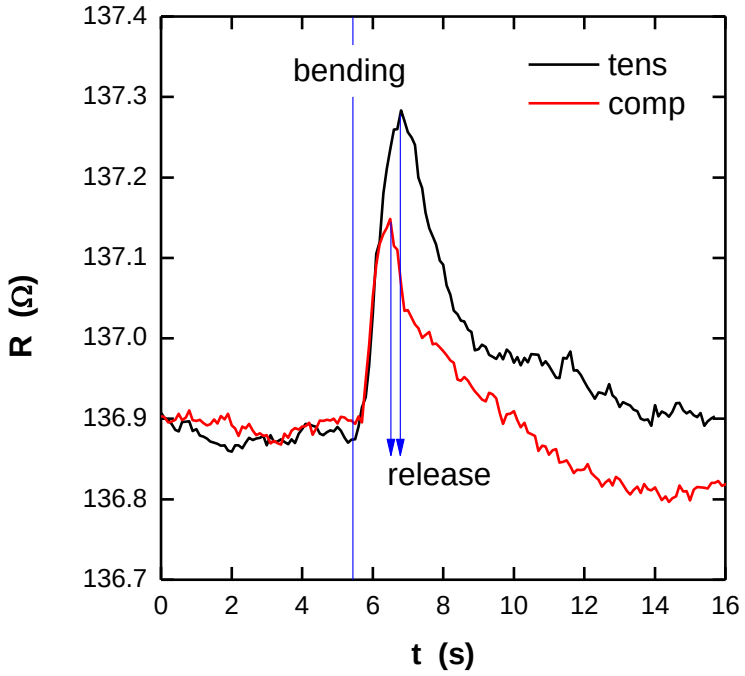

Figure 8. Electrical resistance to applied bending and release.

2.3 Invention of low twist CNT fibers for high performance textiles and composites

The superior mechanical and physical properties of individual CNTs have provided promising opportunities for developing high performance CNT fibers (or fibers), which can be woven or braided into textile structures or directly used as composite reinforcements. This invention involves continuously creating CNT fibers comprising axially aligned and highly packed CNTs without twist or with minimum twist (<15°).

This invention provides an assembly of solutions to current problems in CNT fiber fabrication. Firstly, it improves the productivity of CNT fibers. Low twist ensures better polymer infiltration to the CNT fiber structure and thus enables fast drawing of CNT fibers with good polymer infiltration. In addition, low twist saves time and energy for the fiber spinning process, and therefore makes the resultant CNT fibers appealing for large-scale fabrication and commercial applications. Secondly, since better polymer infiltration is realized and superaligned CNT arrays are used, the low twist CNT fibers produced by this process could have much higher specific modulus and specific strength than those of commercially carbon and synthetic fibers. They could also exhibit high electrical and thermal conductivities, and sensing properties. Thirdly, it is usually difficult to stretch and align the CNTs when the twist angle is above 15°. Low twist provides just enough cohesion and tension for the individual nanotubes, allowing stretching of the CNT fiber possible. The CNTs are stretched and remain continuous when they slide against each other under uniaxial strains. Therefore, long and straight nanotubes become close in contact with each other, which results in effective load transfer. Reduced CNT end clustering would also contribute to the reduced probability of defects and the increase of the composite strength.

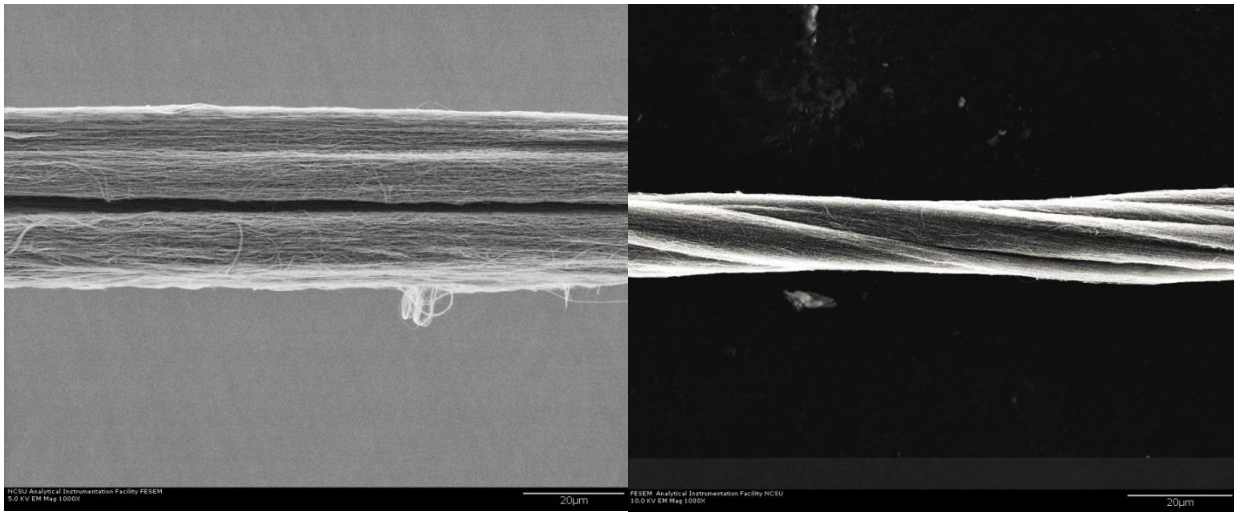

Figure 9. A zero twist fiber (left) and a fiber with 10° twist (right) produced by this invention.

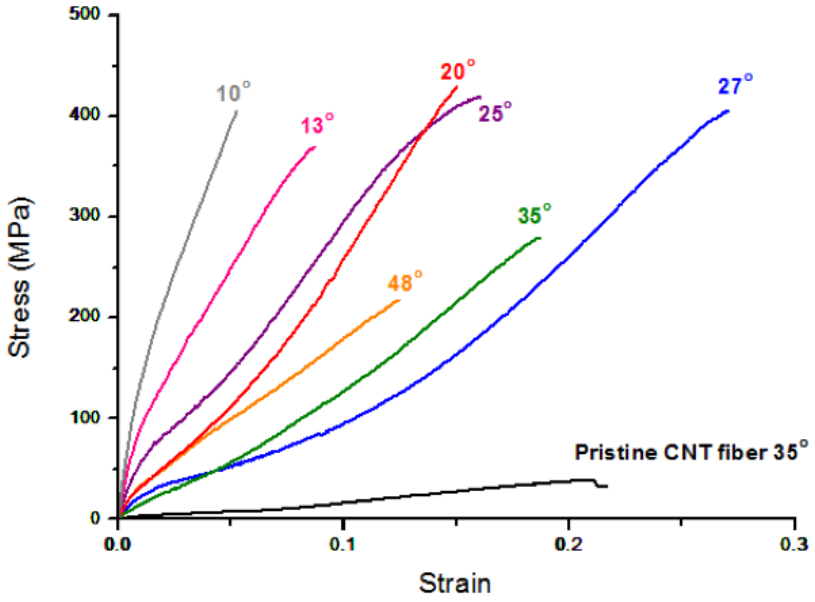

Figure 10. Stress-strain relationship of 0.2% PVA coated CNT fibers with different twist angles

2.4 In-situ strain sensing of glass fiber reinforced composites using embedded flexible twisted CNT fibers under three-point bending

2.4.1 *In Situ* Resistance Behavior of GFRP with CNT Fiber in the Tension Region

When the composite sample was placed in a way that the CNT fiber was near the bottom skin, the CNT fiber deformed in response to the tension force induced by the three-point bending. Five

incremental loading–unloading cycles were applied to the sample, where the deflection of the specimen was controlled to the 20, 40, 60, 80 and 100% of the maximum deflection, corresponding to the 20, 43, 66, 87 and 100% of the fracture stress (tensile strength) of the composite sample, respectively. Figure 11 presents the correlation of nominal mechanical stress and change in electrical resistance ($\Delta R/R$) for the sample. When the GFRP was loaded to 20% of the maximum strain and returned to zero strain, both the nominal stress and electrical resistance change showed linear increase/decrease as the strain increased/decreased. When the GFRP was loaded to 40% and 60%, respectively, of the maximum strain and then unloaded, the nominal stress exhibited linear relationship while the resistance change started to show a flat "loop". The linear increase/decrease of the stress was coming from the GFRP where it has not reached the yielding stage of the matrix. The slight "loop" shown in the resistance change was a consequence of surpassing the elastic deformation of the twisted CNT fiber. Individual nanotubes started to slide against each other, which rendered permanent microstructure change in the fiber. During the 4^{th} load/unload cycle, the trend for electrical resistance change became more obvious. It can be seen that as slippage of nanotubes is prevalent in the fiber structure, the resistance change showed substantial hysteresis in the loading/unloading curves. At the end of the unloaded state, permanent resistance changes of the specimen was observed due to the permanent microstructure change in the CNT fiber.

When the sample was loaded to 100% of the maximum strain, the composite sample yielded and the resistance change of the CNT fiber drastically increased. Finally the electrical resistance became infinite due to sample failure and fiber breakage. Figure 12a is an overview of the five load/unload cycles. It clearly shows the process from linear response to hysteresis for the electrical resistance change in the CNT fiber. Figures 12b shows the change in electrical resistance of the composite during cyclic bending deformation with increasing peak load as a function of time. This self-sensing ability of the GFRP imparts multi-functionality, where the nanotube fiber can detect strains and failure *in situ*. Another advantage of CNT fiber sensor is that it has high electrical conductivity, tailorable structure and resistance, and a hierarchical structure which can effectively sense strain and strain distribution in the host composite.

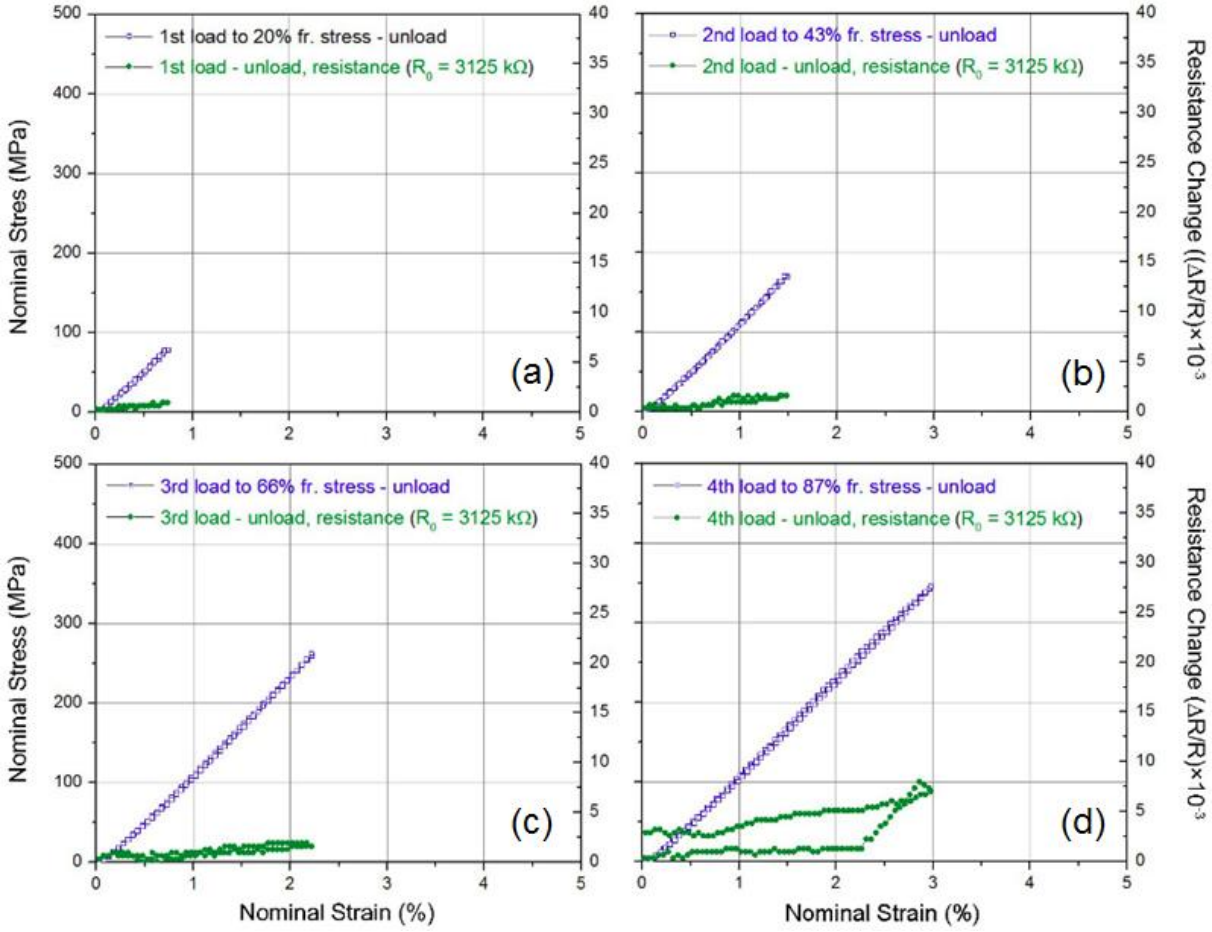

Figure 11. Three-point bending test: mechanical and electrical resistance results of GFRP specimen with embedded CNT fiber in the tension side for four incremental loading-unloading steps.

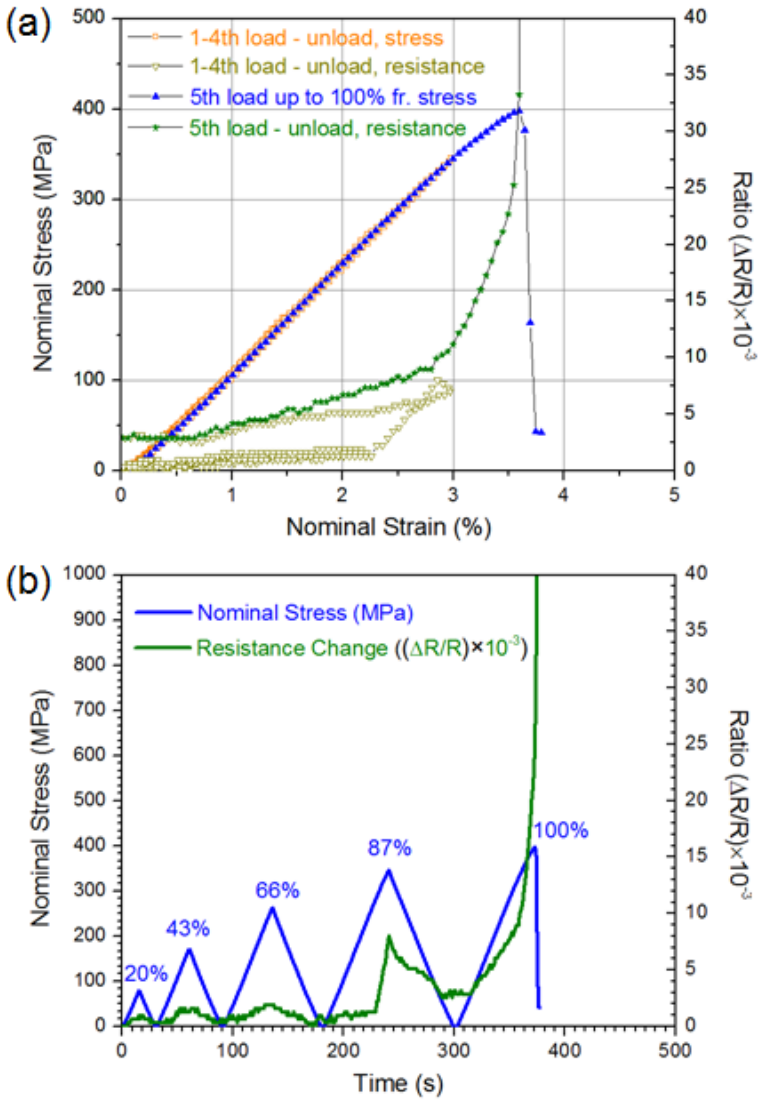

Figure 12. (a) Typical three-point bending test: mechanical and electrical resistance correlation of GFRP specimen with embedded CNT fiber in the tension side for five incremental loading-unloading steps until fracture. (b) Mechanical test procedure and the accompanying resistance response for incremental cyclic loading.

2.4.2 *In Situ* Resistance Behavior of GFRP with CNT Fiber in the Compression Region

When the composite sample was placed in a way that the CNT fiber was near the top skin, the CNT fiber deformed in response to the compression force induced by the three-point bending. During the five load/unload cycles, the resistance change of the CNT fiber first increased then decreased. Figure 13 shows the correlation of nominal mechanical stress and change in electrical resistance (ΔR/R) for the sample. Similar to the test when the CNT fiber was in the tension

region, when the GFRP was loaded to 20% of the maximum strain and returned to zero strain, both the nominal stress and electrical resistance change showed linear increase/decrease as the strain increased/decreased. However, when the GFRP was loaded to 40, 60 and 80%, respectively, of the maximum strain and then unloaded, the electrical resistance started to show a permanent deformation judging from the non-zero returning point on the plots. Permanent deformation in electrical resistance is resulted from slippage of individual nanotubes against each other. The hysteresis in electrical resistance during the 40, 60 and 80% loading-unloading cycles is a direct result of flexural deformation of the CFRP and the CNT fiber. Compared to the fiber embedded at the bottom skin, the CNT fiber at the top skin was subject to a deformation with smaller radius, and thus subject to a larger bending force. Upon unloading of the GFRP, the CNT fiber needed more time and thus generated a hysteresis to return to the original position compared to the fiber at the bottom. Figure 14 shows the mechanical and electrical resistance correlation of GFRP specimen with embedded CNT fiber in the compression side for five incremental loading-unloading steps until fracture. It clearly shows the progression of the permanent deformation and the hysteresis in electrical resistance change of the CNT fiber.

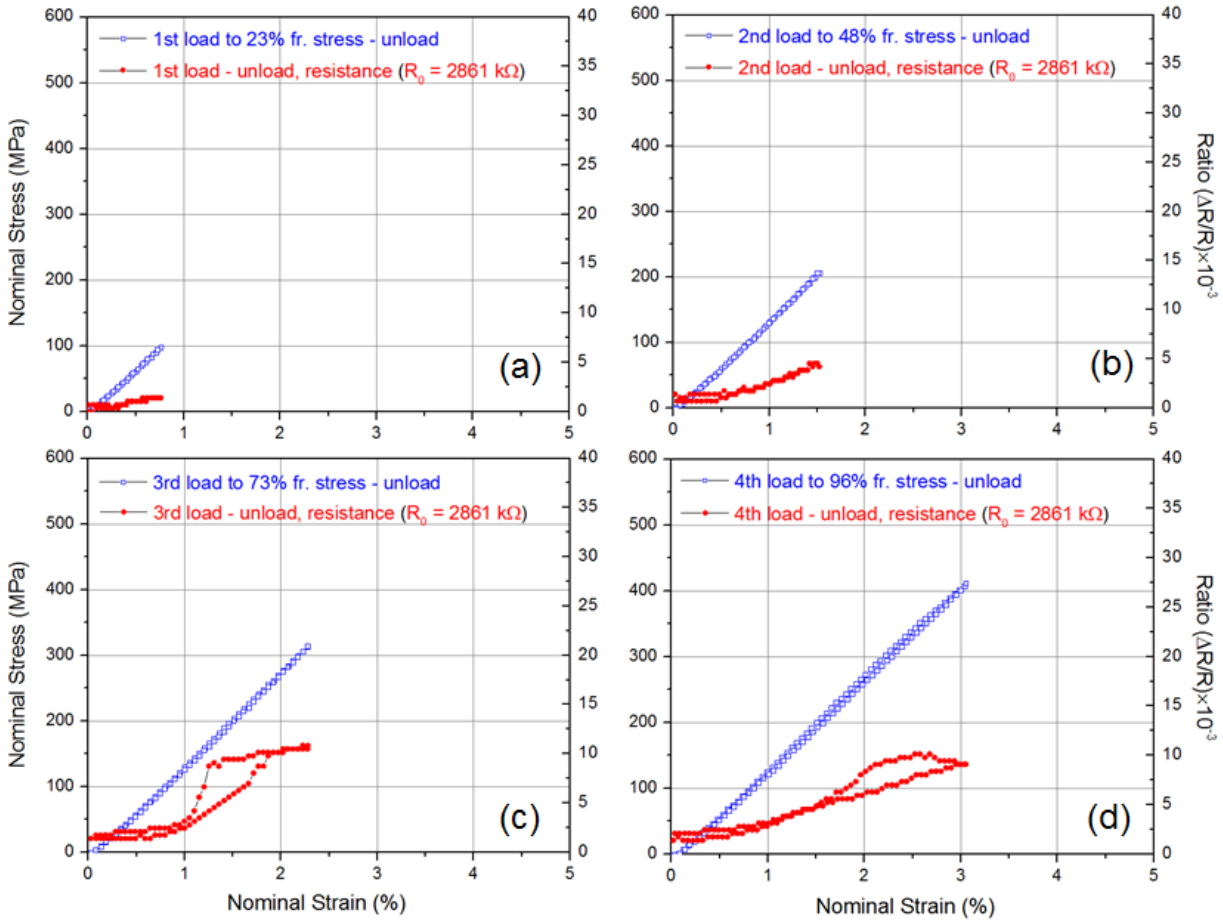

Figure 13. Three-point bending test: mechanical and electrical resistance results of GFRP specimen with embedded CNT fiber in the compression side for four incremental loading-unloading steps.

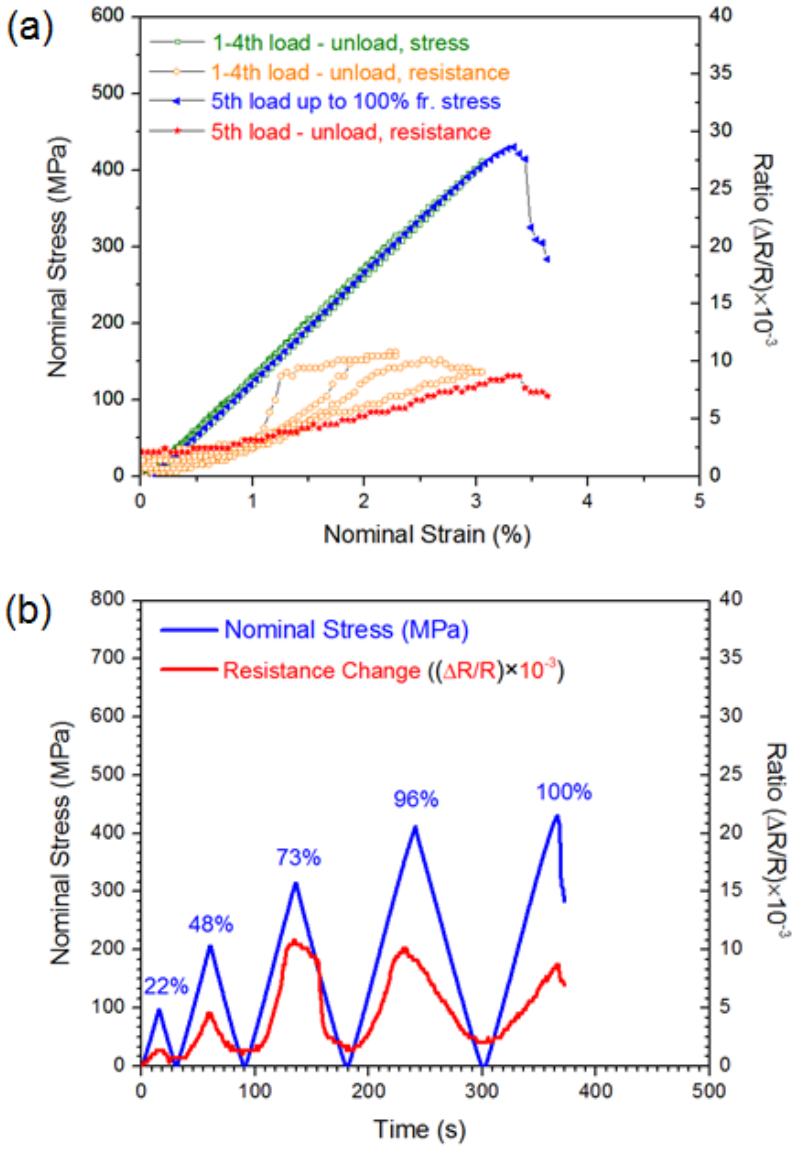

Figure 14. (a) Typical three-point bending test: mechanical and electrical resistance correlation of GFRP specimen with embedded CNT fiber in the compression side for five incremental loading-unloading steps until fracture. (b) Mechanical test procedure and the accompanying resistance response for incremental cyclic loading.

2.5 Four-point bending fatigue test of GFRP material with embedded CNT fiber

Piezoresistive properties of a GFRP with embedded twisted CNT fiber (diameter of ~50 μm, twist angle of ~30°) were obtained upon large cyclic loads (45% and 60% of maximum load, each for 1000 cycles, respectively) under four-point flexural tests at 0.5 Hz. The corresponding variations in electric resistance and the load cycles are reported in Figure 15.

Overall the test results suggest that the twisted CNT fiber has the capability to sense strains in terms of flexural loadings up to 60% of maximum load. It is advantageous over fibers made with dispersed short CNTs, because dispersed short CNTs cannot withstand large strains due to contact lost. During the first 1000 cycles at 45% of maximum load, the electrical resistance change of the GFRP is slightly larger at the initial stage of the cycling test (initial stage in Figure 15), which indicates that pre-cycling may allow the carbon nanotubes to straighten and realign themselves under strains. After pre-cycling, the resistance became stable at 45% of maximum load, since the nanotubes now have stable contact with each other.

When larger load was applied (60% of maximum load), the electrical resistance change of the CFRP first increased then decreased. This could be due to further slippage of nanotubes against each other, which makes the CNT fiber exhibit a behavior similar to the viscoelastic properties of polymer materials. Under repeated elongations of the composite with embedded CNT fiber during the 1000 cycles at 60% of maximum load, R/R_0 slightly drifts downward then upward, which is attributed to the CNT fiber structure rearrangement. After each cycle, the electrical resistance does not go back to its initial value, indicating that phenomena occurring in the fiber permanently modify the morphology of the CNTs. It is expected that higher test loadings would affect more deeply the strain accumulated in the fiber and thus its structure.

From the flexural fatigue tests a relation between piezoresistive effects and stress/strain is established: the R/R_0 changes are proportional to the tensile stress with synchronous variations and a large signal/noise ratio. Future work includes testing at larger loadings (75%) until composite fracture, and identifying the onset of crack initiation and propagation in the composite structure, by analyzing the resistance response of the embedded CNT fiber. The technique of using embedded twisted CNT fiber to sense the damage in the composite materials *in-situ* will also be verified with microscopy examinations.

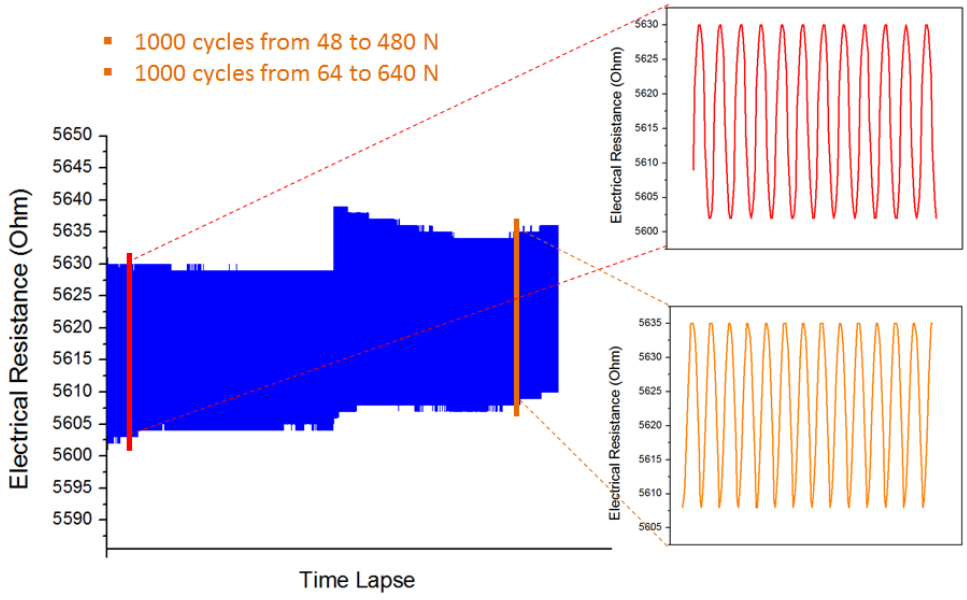

Figure 15. Piezoresistive variations of the CNT fiber embedded GFRP upon four point flexural fatigue tests at 0.5 Hz

2.6 Oxygen plasma treatment of raw CNT ribbons that are used to fabricate CNT fibers

Utilizing spinnable CNTs to produce high-strength CNT fibers has been considered an effective route to develop the next-generation CNT fiber composites. However, the reported tensile strengths of the as-prepared fibers are far below that of an individual CNT. It is believed that nanotube slippage against each other results in the lower strength. When fabricating CNT fiber composites, the lack of interfacial bonding between CNTs and the polymer matrix also leads to lower-than-predicted mechanical properties. Here we used oxygen plasma to treat the as-synthesized CNT array, and then improved the resulting tensile strength of CNT/Bismaleimide composites by 82%, and Young's modulus by 26%. This method is going to be applied to fabricating CNT fibers and CNT fiber composites.

Table 1. Mechanical properties of composites fabricated by non-treated CNTs and plasma treated CNTs.

Sample	Tensile Strength (MPa)	Young's Modulus (GPa)	Strain-to-failure (%)
Non treated CNT/2.5 g L^{-1} BMI	337±45 (384)	25.4±4.3	2.0±0.3
Plasma treated CNT/2.5 g L^{-1} BMI	613±77 (810)	32.0±2.2	3.1±0.4

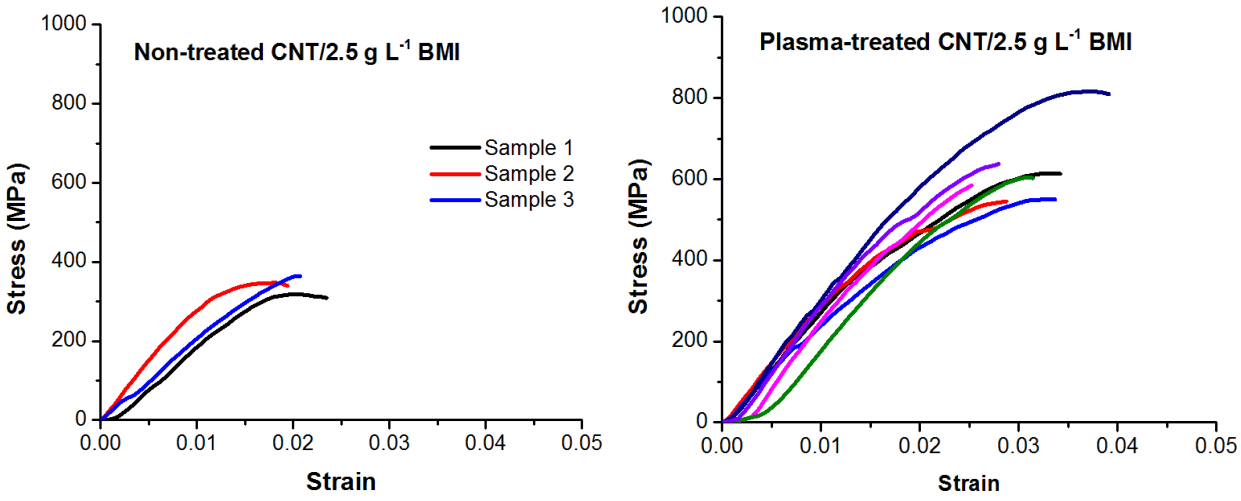

Figure 16. Tensile stress-strain curves of composites fabricated by non-treated CNTs (left) and plasma treated CNTs (right).

Summary:

In this project, the Co-PI's (Prof. Zhu) group has palyed a supporting role to the fundamental research by the PI's (Prof. Chou) group. In that role, we (the Co-PI's group) have fabbricated CNT fibers, composite samples, and CNT-fiber sensors embedded in composite, as requested by the PI's group. Only some of these samples produced meaningful scientific data for publications, as expected in experimental studies.

In this process, we have also developed/optimized parameters to synthesize spinnable CNT arrays with consistent quality, and designed and made in house the automatic machinces/devices for fabricating the CNT fibers and composites.

We have also made the following notable researches/achievements, some of which are being writen up for publications (listed in a later section):

- Disclosed one patent on low-twist CNT fibers
- In-situ strain sensing of glass fiber reinforced composites using embedded flexible twisted CNT fibers under three-point bending
- Four-point bending fatigue test of GFRP material with embedded CNT fiber
- Oxygen plasma treatment of raw CNT ribbons that are used to fabricate CNT fibers

References:

[1]. M. Zu, Q. W. Li, Y. T. Zhu, M. Dey, G. J. Wang, W. B. Lu, J. M. Deitzel, J. W. Gillespie Jr., J. -H. Byun and T. -W. Chou. The effective interfacial shear strength of carbon nanotube fibers in an epoxy matrix characterized by a microdroplet test, Carbon, 50, 1271–1279, 2012.

[2]. M. Zu, Q. W. Li, Y. T. Zhu, Y. Zhu, G. J. Wang, J. -H. Byun and T. -W. Chou. Stress relaxation in carbon nanotube-based fibers for load-bearing applications, Carbon, 52, 347–355, 2012.

[3]. A.S. Wu, L. Zhang, Y.T. Zhu, T.W. Chou, Sensing strain under bending and tension in carbon nanotube fiber composites, Carbon Letter, submitted.

[4]. X. Wang, H. West, Y.T. Zhu, T.W. Chou, In-situ Strain Sensing of Glass Fiber Reinforced Composites using Embedded Flexible Twisted CNT Fibers, 2014, in preparation.

[5]. Y.T. Zhu, C. Page, L. Zhang, X. Wang, Low twist CNT yarns for high performance textiles and composites patent, NCSU disclosure # 11014, 2012.

[6] Y. Inoue, K. Kakihata, Y. Hirono, T. Horie, A. Ishida, H. Mimura, One-step grown aligned bulk carbon nanotubes by chloride mediated chemical vapor deposition. Appl Phys Lett 2008;92:213113.

Personnel Supported:

Yuntian Zhu, Co-Principal Investigator

Xin Wang, Postdoc Research Scholar

Liwen Zhang, graduate student

Journal Publications of the Co-PI's Research Group During the Grant Period:

1. M. Zu, Q. W. Li, Y. T. Zhu, M. Dey, G. J. Wang, W. B. Lu, J. M. Deitzel, J. W. Gillespie Jr., J. -H. Byun and T. -W. Chou. The effective interfacial shear strength of carbon nanotube fibers in an epoxy matrix characterized by a microdroplet test, *Carbon*, **50**, 1271–1279, 2012.
2. M. Zu, Q. W. Li, Y. T. Zhu, Y. Zhu, G. J. Wang, J. -H. Byun and T. -W. Chou. Stress relaxation in carbon nanotube-based fibers for load-bearing applications, Carbon, 52, 347–355, 2012.
3. X. Wang, H. West, Y.T. Zhu, T.W. Chou, In-situ Strain Sensing of Glass Fiber Reinforced Composites using Embedded Flexible Twisted CNT Fibers, 2014, in preparation.
4. Y.T. Zhu, C. Page, L. Zhang, X. Wang, Low twist CNT yarns for high performance textiles and composites patent, NCSU disclosure # 11014, 2012.

Papers plan to write for the research work funded by this Grant:

1. Mechanical Property Improvement of CNT/BMI Fibers by Oxygen Plasma Treatment of CNT Arrays, 2014
2. Electrical Conductivity Enhancement in Carbon Nanotube Fibers by Doping, 2014

Honors/Awards (Yuntian Zhu):

2011 Fellow, American Physical Society
2012 Fellow, American Association for the Advancement of Science (AAAS)
2012 TMS SMD Distinguished Scientist/Engineer Award
2014 Albert Sauveur Achievement Award, ASM International
2014 Alcoa Foundation Distinguished Engineering Research Award, NC State University
2014 Highly Cited Researchers 2014, Thomson Reuters (ISI).

Prior to Current Grant Period (Yuntian Zhu):

1999 Achievement Award, Los Alamos National Laboratory
2005 Nano50 Award, 4-cm Long Carbon Nanotubes, by *Nanotech Briefs*
2006 Best Idea Award, Los Alamos National Lab.
2007 Nano50 Award, The Ultra-Strong, Stiff, and Lightweight CNT Fiber, by *Nanotech Briefs*
2010 Fellow, ASM International
2010 TMS MPMD Distinguished Scientist/Engineer Award
2010 Alumni Outstanding Research Award, NC State University
2010 Thousand Plan Scholar, China